Electronic Supplementary Information

Stabilization and Reactivity Studies of Donor-Base Ligands-Supported Gallium-Phosphides with Stronger Binding Energy: A Theoretical Approach

Maria Francis,[a] Sudipta Roy*,[a]

[a]Department of Chemistry, Indian Institute of Science Education and Research (IISER) Tirupati, Tirupati, 517507, India.

Email: roy.sudipta@iisertirupati.ac.in

Table of Contents

Figure S5. The LUMO, HOMO, HOMO-1 and HOMO-2 of **8** at BP86-D3(BJ)/def2-TZVPP level. Energies are in kcal/mol.

Figure S6. Optimized geometries of compounds **9** in singlet ground state at BP86-D3(BJ)/def2-TZVPP level of theory.

Figure S7. The LUMO, HOMO, HOMO-1 and HOMO-2 of **9** at BP86-D3(BJ)/def2-TZVPP level. Energies are in kcal/mol.

Table S8. NBO results of the compound $(cAAC)_2GaP\text{-}Ni(CO)_3$ (**9**) at the BP86-D3(BJ)/def2-TZVPP level of theory.

Figure S8. Contour plots of Laplacian distribution [$\nabla^2\rho(r)$] in the P-Ga-L′ plane of compounds **1**-**7**.

Table S9. EDA-NOCV results of L–PGa–L′, bonds of L-P-Ga-L′ [L, L′ = $cAAC^{Me}$ (**1**), L = cAAC, L′ = NHC^{Me} (**2**), L = cAAC, L′ = PMe_3 (**3**), L = NHC, L′ = cAAC (**4**), L = NHC, L′ = PMe_3 (**5**), L, L′ = NHC^{Me} (**6**), L, L′ = PMe_3 (**7**)].

Table S10. The EDA-NOCV results at the BP86-D3(BJ)/TZ2P level of L–PGa–L′ bonds of L-P-Ga-L′ [L = $cAAC^{Me}$, L′ = PMe_3 (**3**); L, L′ = PMe_3 (**7**)] complexes using [ligands]$^+$ and [P-Ga]$^-$ in the electronic doublet (D) states as interacting fragments. Energies are in kcal/mol.

Figure S9. The shape of the deformation densities $\Delta\rho_{(1)\text{-}(4)}$ that correspond to $\Delta E_{orb(1)\text{-}(4)}$, and the associated MOs of cAAC-P-Ga-NHC (**2**) and the fragments orbitals of [(cAAC) (NHC)] and [P-Ga] in the Singlet state (S) at the BP86-D3(BJ)/TZ2P level.

Figure S10. The shape of the deformation densities $\Delta\rho_{(1)\text{-}(3)}$ that correspond to $\Delta E_{orb(1)\text{-}(3)}$, and the associated MOs of cAAC-P-Ga-PMe_3 (**3**) and the fragments orbitals of [(cAAC) $(PMe_3)]^+$ and [P-Ga]$^-$ in the doublet state (D) at the BP86-D3(BJ)/TZ2P level.

Figure S11. The shape of the deformation densities $\Delta\rho_{(1)\text{-}(4)}$ that correspond to $\Delta E_{orb(1)\text{-}(4)}$, and the associated MOs of NHC-P-Ga-cAAC (**4**) and the fragments orbitals of [(NHC) (cAAC)] and [P-Ga] in the Singlet state (S) at the BP86-D3(BJ)/TZ2P level.

Figure S12. The shape of the deformation densities $\Delta\rho_{(1)\text{-}(4)}$ that correspond to $\Delta E_{orb(1)\text{-}(4)}$, and the associated MOs of NHC-P-Ga-NHC (**6**) and the fragments orbitals of $[(NHC)_2]$ and [P-Ga] in the Singlet state (S) at the BP86-D3(BJ)/TZ2P level.

Figure S13. The shape of the deformation densities $\Delta\rho_{(1)\text{-}(3)}$ that correspond to $\Delta E_{orb(1)\text{-}(3)}$, and the associated MOs of PMe_3-P-Ga-PMe_3 (**7**) and the fragments orbitals of $[(PMe_3)\ (PMe_3)]^+$ and [P-Ga]$^-$ in the doublet state (D) at the BP86-D3(BJ)/TZ2P level.

Table S11. The EDA-NOCV results at the M06-2X/TZ2P level of L–PGa–L′ bonds of L-P-Ga-L′ complex [L, L′ = $cAAC^{Me}$ (**1**), L = $cAAC^{Me}$, L′ = NHC^{Me} (**2**), L = NHC^{Me}, L′ = $cAAC^{Me}$ (**4**), L, L′ = PMe_3 (**7**)] using [ligands] and [P-Ga] in the electronic singlet (S) states as interacting fragments. Energies are in kcal/mol.

Table S12. EDA-NOCV results of (L)P–Ga(L′) bond of L-P-Ga-L′ [L, L′ = $cAAC^{Me}$ (**1**), L = cAAC, L′ = NHC^{Me} (**2**), L = cAAC, L′ = PMe_3 (**3**), L = NHC, L′ = cAAC (**4**), L = NHC, L′ = PMe_3 (**5**), L, L′ = NHC^{Me} (**6**), L, L′ = PMe_3 (**7**)] complexes using three different sets of fragments with different charges and electronic states (S = singlet, D = doublet) and associated bond types at the BP86-D3(BJ)/TZ2P level.

Table S13. The EDA-NOCV results of P−Ga bond of compounds **1** and **2** at the BP86-D3(BJ)/TZ2P level. Energies are in kcal/mol.

Table S14. The EDA-NOCV results of P−Ga bond of compounds **3**-**7** at the BP86-D3(BJ)/TZ2P level. Energies are in kcal/mol.

Figures S14-S20. The shape of the deformation densities $\Delta\rho_{(1)-(2)}$ that correspond to $\Delta E_{orb(1)-(2)}$, and the associated MOs of compounds **1**-**7** at the BP86-D3(BJ)/TZ2P level.

Table S15. EDA-NOCV results of NHC^{DMP}-P-Ga-NHC^{DMP} (**6′**) using two different sets of fragments with different charges and electronic states (S = singlet, D = doublet) and associated bond types at the BP86-D3(BJ)/TZ2P level.

Table S16. The EDA-NOCV results at the BP86-D3(BJ)/TZ2P level of L–PGa–L′ bonds of NHC^{DMP}-P-Ga-NHC^{DMP} (**6′**) using [ligands] and [P-Ga] in the electronic singlet (S) states as interacting fragments. Energies are in kcal/mol.

Figure 21. The shape of the deformation densities $\Delta\rho_{(1)-(4)}$ that correspond to $\Delta E_{orb(1)-(4)}$, and the associated MOs of NHC^{DMP}-P-Ga-NHC^{DMP} (**6′**) and the fragments orbitals of [$(NHC^{DMP})_2$] and [P-Ga] in the Singlet state (S) at the BP86-D3(BJ)/TZ2P level.

Table S17. EDA-NOCV results of $(cAAC)_2GaP{-}Fe(CO)_4$ bond of $(cAAC)_2GaP$-$Fe(CO)_4$ (**8**) complex using three different sets of fragments with different charges and electronic states (S = singlet, D = doublet, T = triplet) and associated bond types at the BP86-D3(BJ)/TZ2P level.

Table S18. The EDA-NOCV results at the BP86-D3(BJ)/TZ2P level of $(cAAC)_2GaP$ - $Fe(CO)_4$ bond of $(cAAC)_2GaP$-$Fe(CO)_4$ (**8**) complex using [$(cAAC)_2GaP$] and [$Fe(CO)_4$] in the electronic singlet (S) states as interacting fragments. Energies are in kcal/mol.

Figure 22. The shape of the deformation densities $\Delta\rho_{(1)-(4)}$ that correspond to $\Delta E_{orb(1)-(2)}$, and the associated MOs of $(cAAC)_2GaP{-}(Fe(CO)_4$ (**8**) and the fragments orbitals of $(cAAC)_2GaP$ and [$(Fe(CO)_4$] in the Singlet state (S) at the BP86-D3(BJ)/TZ2P level.

Table S19. EDA-NOCV results of $(cAAC)_2GaP{-}Ni(CO)_3$ bond of $(cAAC)_2GaP$-$Ni(CO)_3$ (**9**) complex using three different sets of fragments with different charges and electronic states (S = singlet, D = doublet, T = triplet) and associated bond types at the BP86-D3(BJ)/TZ2P level.

Table S20. The EDA-NOCV results at the BP86-D3(BJ)/TZ2P level of $(cAAC)_2GaP{-}Ni(CO)_3$ bond of $(cAAC)_2GaP{-}Ni(CO)_3$ (**9**) complex using [$(cAAC)_2GaP$] and [$Ni(CO)_3$] in the electronic singlet (S) states as interacting fragments. Energies are in kcal/mol.

Figure 23. The shape of the deformation densities $\Delta\rho_{(1)-(4)}$ that correspond to $\Delta E_{orb(1)-(2)}$, and the associated MOs of $(cAAC)_2GaP{-}Ni(CO)_3$ (**9**) and the fragments orbitals of $(cAAC)_2GaP$ and [$Ni(CO)_3$] in the Singlet state (S) at the BP86-D3(BJ)/TZ2P level.

Table S21. The EDA-NOCV results at the M06-2X/TZ2P level for $(cAAC)_2GaP{-}M(CO)_n$ bond of $(cAAC)_2GaP{-}M(CO)_n$ complex [M = Fe, n = 4 (**8**); M = Ni, n = 3 (**9**)] using [$(cAAC)_2GaP$] and [$M(CO)_n$] in the electronic singlet (S) states as interacting fragments. Energies are in kcal/mol.

Table S22. NBO results of the compound NHC^{DMP}–P–Ga–NHC^{DMP} (**6′**) at the BP86-D3(BJ)/def2-TZVPP level of theory.

Table S23. NBO results of compounds **1**-**7** at the B3LYP/def2-TZVPP level of theory.

Table S24. NBO results of compounds **1**-**7** at the M06-2X/def2-TZVPP level of theory.

Computational Methods:

The geometry optimisations and frequency calculations of compounds **1**-**7** with general formula L-PGa-L′ [L, L′ = $cAAC^{Me}$ (**1**); L = $cAAC^{Me}$, L′ = NHC^{Me} (**2**); L = $cAAC^{Me}$, L′ = PMe_3 (**3**); L = NHC^{Me}, L′ = $cAAC^{Me}$ (**4**); L = NHC^{Me}, L′ = PMe_3 (**5**); L, L′ = NHC^{Me} (**6**); L, L′ = NHC^{DMP} (DMP = 2,6-dimethylphenyl) (**6′**); L, L′ = PMe_3 (**7**)] and **8**-**9** with general formula $(cAAC)_2GaP\text{-}MCO_n$ [M = Fe; n = 4 (**8**), M = Ni; n = 3 (**9**)] were performed at BP86/def2-TZVPP, B3LYP/def2-TZVPP (hybrid functional), and M06-2X/def2-TZVPP (meta-hybrid functional)[1] levels using Gaussian 16.[2] The absence of imaginary frequency indicates that the optimised molecules are at the minima of the potential energy surfaces. The Wiberg bond indices (WBI), occupation numbers (ON), partial charges (q) on the atoms, and natural bond orbitals have all been evaluated using the NBO 6.0 programme[3] on the above mentioned three levels. Wavefunction generation were performed using the BP86/def2-TZVPP and M06-2X/def2-TZVPP levels of theory and basis set. Laplacian of electron density were generated using AIMALL software package.[4]

Method Calibration: The structural parameters of equilibrium geometries for compounds **1**-**7** are found to be slightly different in three level of theories. The singlet-triplet energy gaps of **1**-**7** with M06-2X functional are found to be in between to those values calculated with B3LYP, and M06-2X functionals. The dissociation energies of **1**-**6′** are found to be close to each other with B3LYP, and M06-2X functionals. The studies conducted by G. Frenking isoelectronic homologues of carbones, CL_2,[5] when the ligands were CO and N_2, they could observe considerable difference between theoretically predicted BDE using pure and hybrid GGA functional such as BP86, B3LYP, and *ab initio* data at the CCSD(T) and SCS-MP2. But this abnormality was not observed when ligands were PPh_3, NHC and cAAC. Comparable results were obtained for ligands CO and N_2 when meta-GGA functional M05-2X was used. The calculations performed at BP86 for the bulkier ligands like PPh_3, NHC and cAAC were consistent with the calculations performed at SCS-MP2 and M05-2X. In the light of the studies conducted by Frenking and group, we performed our studies in pure GGA (BP86), hybrid GGA (B3LYP), and meta-GGA (M06-2X) functionals.

Results:

Table S1. Energy difference ($\Delta E_{Singlet\text{-}Triplet}$) between singlet and triplet states calculated with BP86, B3LYP, and M06-2X functionals. Energy values are in kcal/mol.

Compound	**BP86**	**B3LYP**	**M06-2X**
cAAC-PGa-cAAC (**1**)	12.66	13.96	9.18
cAAC-PGa-NHC (**2**)	18.83	21.68	15.78
cAAC-PGa-PMe_3 (**3**)	26.32	29.09	24.22
NHC-PGa-cAAC (**4**)	16.75	17.46	12.09
NHC-PGa-PMe_3 (**5**)	33.16	34.84	29.30
NHC-PGa-NHC (**6**)	24.76		19.29
NHC^{DMP}-PGa-NHC^{DMP} (**6′**)	26.07	28.04	18.02
PMe_3-PGa-PMe_3 (**7**)	32.75	35.33	28.77

Multiple attempts to optimize Compound **6** failed in triplet state, so we could not calculate the energy difference between singlet and triplet states with B3LYP functional.

Table S2. Bond dissociation energies (BDE) (kcal/mol) of L-PGa-L′ bonds of compounds **1-9** calculated with M06-2X, BP86, and B3LYP functionals.

Compound	**Dissociation energy**		
	M06-2X	**BP86**	**B3LYP**
cAAC-PGa-cAAC (**1**)	125.38	137.09	128.86
cAAC-PGa-NHC (**2**)	120.1	128.91	122.29
cAAC-PGa-PMe_3 (**3**)	111.67	119.71	113.71
NHC-PGa-cAAC (**4**)	111.28	118.35	110.99
NHC-PGa-PMe_3 (**5**)	98.563	106.09	100.32
NHC-PGa-NHC (**6**)	105.04	110.53	
NHC^{DMP}-PGa-NHC^{DMP} (**6′**)	108.42	126.06	114.56
PMe_3-PGa-PMe_3 (**7**)	87.644	93.96	89.44
$(cAAC)_2GaP$-$(Fe(CO)_4)$ (**8**)	35.69	51.19	61.40
$(cAAC)_2GaP$-$(Ni(CO)_3)$ (**9**)	18.64	31.12	39.79

Table S3. Energies (in kcal/mol) of selected molecular orbitals with BP86, B3LYP, and M06-2X functionals for the compounds **1-9**.

	LUMO			**HOMO**			**HOMO-1**			**HOMO-2**		
	BP86	B3LYP	M06-2X	BP86	B3LYP	M06-2X	BP86	B3LYP	M06-2X	BP86	B3LYP	M06-2X
1	-35.97	-17.99	-2.54	-74.95	-84.86	-109.53	-92.93	-103.54	-127.29	-112.53	-128.44	-155.89
2	-36.43	-18.91	-1.15	-72.18	-82.55	-105.15	-90.63	-102.16	-128.44	-117.14	-133.98	-159.81
3	-42.66	-27.21	-8.99	-80.48	-91.78	-115.76	-95.47	-107.92	-133.98	-122.91	-139.97	-166.03
4	-33.44	-15.68	6.23	-74.02	-82.79	-105.38	-83.25	-92.70	-116.91	-106.77	-124.29	-150.58
5	-28.13	-12.68	5.30	-81.17	-91.32	-113.69	-87.4	-98.24	-124.29	-116.68	-133.52	-159.34
6	-25.83	-9.22	8.30	-77.71	-86.94	-107.92	-83.02	-92.93	-117.61	-105.15	-121.07	-145.51
6′	-33.44	-13.84	6.69	-75.64	-83.48	-103.77	-82.55	-91.78	-116.22	-113.92	-130.52	-156.81
7	-34.82	-19.14	-0.23	-86.94	-98.01	-121.526	-94.78	-106.54	-134.44	-124.75	-141.82	-168.8
8	-52.12	-33.21	-10.83	-92.7	-102.6	-123.14	-109.8	-112.53	-133.52	-134.44	-122.68	-151.5
9	-50.96	-32.74	-10.38	-91.55	-100.5	-118.07	-98.01	-109.3	-133.52	-118.99	-133.75	-157.73

Table S4. Energies (in kcal/mol) of HOMO-LUMO gap with BP86, B3LYP, and M06-2X functionals for the compounds **1-9**.

Compound	**BP86**	**B3LYP**	**M06-2X**
cAAC-PGa-cAAC (**1**)	38.97	66.87	107
cAAC-PGa-NHC (**2**)	35.74	63.65	104
cAAC-PGa-PMe_3 (**3**)	37.82	64.57	106.77

NHC-PGa-cAAC (**4**)	40.59	67.1	111.61
NHC-PGa-PMe_3 (**5**)	53.04	78.63	118.99
NHC-PGa-NHC (**6**)	51.89	77.71	116.22
PMe_3-PGa-PMe_3 (**7**)	52.12	78.87	121.3
NHC^{DMP}-PGa-NHC^{DMP} (**6′**)	42.2	69.64	110.46
$(cAAC)_2GaP$-$(Fe(CO)_4)$ (**8**)	40.59	69.41	112.3
$(cAAC)_2GaP$-$(Ni(CO)_3)$ (**9**)	40.59	67.8	107.69

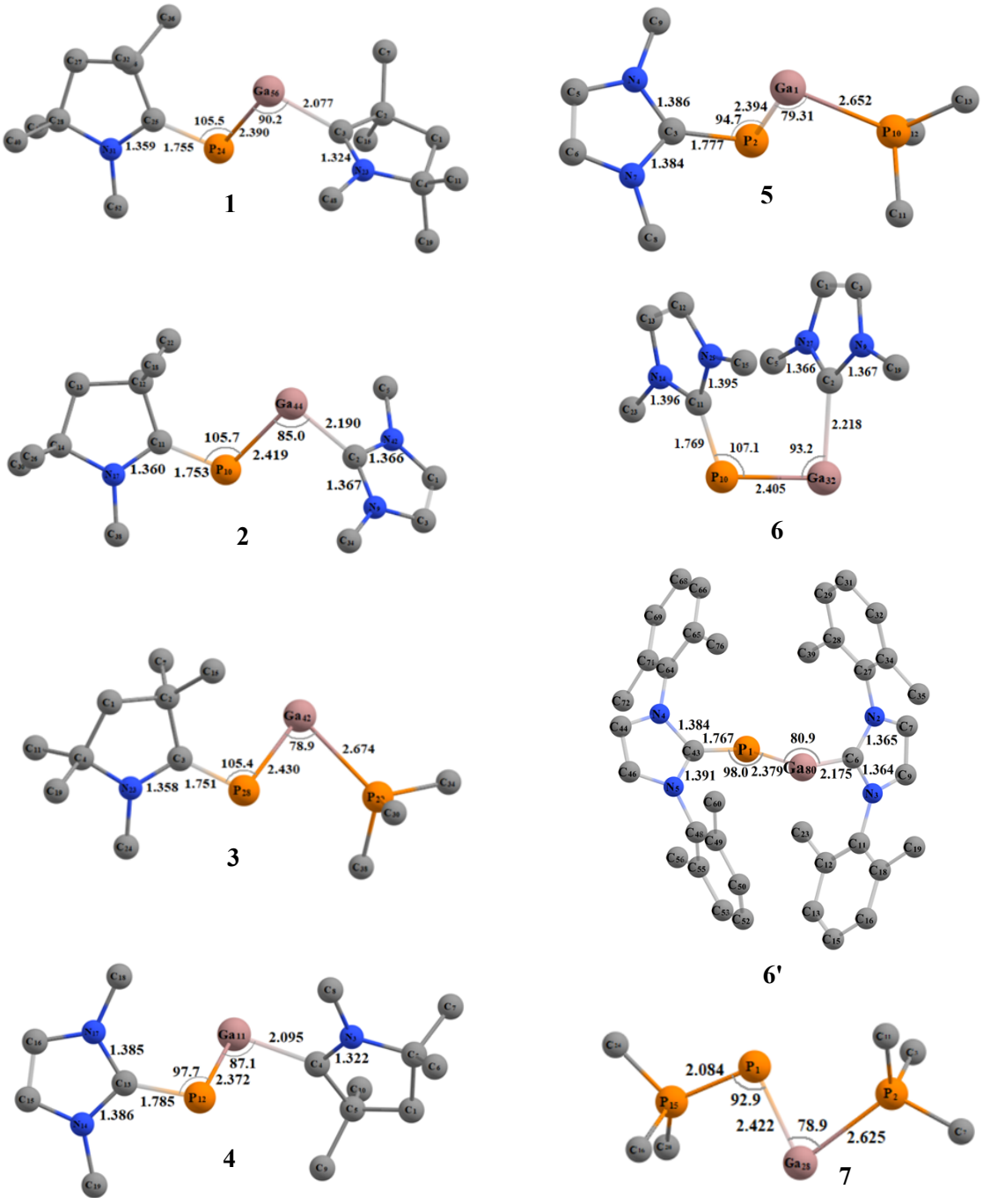

Figure S1. Optimized geometries of compounds **1** to **7** in singlet ground state with L, L′ = cAAC^{Me} (**1**); L = cAAC^{Me}, L′ = NHC^{Me} (**2**); L = cAAC^{Me}, L′ = PMe_3 (**3**); L = NHC^{Me}, L′ = cAAC^{Me} (**4**); L = NHC^{Me}, L′ = PMe_3 (**5**); L, L′ = NHC^{Me} (**6**); L, L′ = NHC^{DMP} (DMP = 2,6-dimethylphenyl) (**6′**); L, L′ = PMe_3 (**7**) at BP86-D3(BJ)/def2-TZVPP level of theory.

Table S5. Selected bond lengths (Å) of **1**-**9**.

Compound	Bond	BP86	B3LYP	M06-2X
1	C25-P24	1.755	1.744	1.732
	P24-Ga56	2.390	2.430	2.476
	Ga56-C3	2.077	2.136	2.191
	N31-C25	1.359	1.352	1.352
	N23-C3	1.324	1.306	1.298
2	C11-P10	1.753	1.744	1.742
	P10-Ga44	2.419	2.437	2.454
	Ga44-C2	2.190	2.230	2.234
	N17-C11	1.360	1.353	1.349
	N9-C2	1.367	1.354	1.346
	N42-C2	1.366	1.354	1.347
3	C3-P28	1.751	1.743	1.742
	P28-Ga42	2.430	2.442	2.436
	Ga42-P29	2.674	2.747	2.749
	C3-N23	1.358	1.351	1.346
4	C13-P12	1.785	1.777	1.783
	P12-Ga11	2.372	2.394	2.418
	Ga11-C4	2.095	2.138	2.175
	N17-C13	1.385	1.377	1.367
	N14-C13	1.386	1.376	1.367
	N3-C4	1.322	1.306	1.299
5	C3-P2	1.777	1.777	1.784
	P2-Ga1	2.394	2.394	2.387
	Ga1-P10	2.652	2.711	2.714

	N7-C3	1.384	1.373	1.364
	N4-C3	1.386	1.374	1.366
6	C11-P10	1.769	1.766	1.770
	P10-Ga32	2.405	2.412	2.413
	Ga32-C11	2.218	2.268	2.280
	N14-C11	1.394	1.383	1.376
	N29-C11	1.395	1.384	1.376
	N9-C2	1.367	1.356	1.354
	N27-C2	1.366	1.355	1.354
7	P15-P1	2.084	2.078	2.076
	P1-Ga28	2.422	2.423	2.409
	Ga28-P2	2.625	2.683	2.688
6′	C43 – P1	1.767	1.761	1.767
	P1 – Ga80	2.379	2.383	2.403
	Ga80 – C6	2.175	2.221	2.251
	C43 – N4	1.384	1.377	1.372
	C43 – N5	1.391	1.381	1.373
	C6 – N2	1.365	1.355	1.351
	C6 – N3	1.364	1.355	1.351
8	C3 – P64	1.770	1.761	1.758
	P64 – Ga65	2.381	2.420	2.436
	P64 – Fe55	2.350	2.383	2.445
	Ga65 – C24	2.113	2.157	2.170
	C24 – N30	1.459	1.299	1.297
	C3 – N23	1.345	1.337	1.338
9	C3 – P62	1.758	1.749	1.750

	P62 – Ni55	2.330	2.363	2.476
	P62 – Ga63	2.398	2.421	2.432
	Ga63 – C24	2.135	2.173	2..190
	C24 – N30	1.312	1.299	1.297
	C3 – N23	1.350	1.343	1.340

Table S6. Selected bond angles (º) of **1-9**.

Compound	**Bond Angle**	**BP86**	**B3LYP**	**M06-2X**
1	C25 – P24 - Ga56	105.5	107.2	109.8
	C3 – Ga56 – P24	90.2	85.2	77.5
2	C2 – Ga44 – P10	85.0	83.8	78.2
	Ga44 – P10 – C11	105.7	107.3	109.5
3	C3 – P28 – Ga42	105.4	106.6	107.4
	P28 – Ga42 – P29	78.9	79.2	78.4
4	C4 – Ga11 – P12	87.1	84.3	78.0
	C13 – P12 – Ga11	97.7	101.7	100.4
5	C3 – P2 – Ga1	94.7	96.2	95.6
	P2 – Ga1 – P10	79.3	80.2	79.3
6	C2 – Ga32 – P10	93.2	2.268	96.4
	C11 – P10 – Ga32	107.1	107.5	110.5
7	P2 - Ga28 – P1	78.9	79.8	79.9
	P15 – P1 – Ga28	92.9	94.6	93.8
6′	C43 – P1 – Ga80	98.0	101.7	105.2
	P1 – Ga80 – C6	80.9	81.8	80.1
8	C24 – Ga65 – P64	93.7	92.2	92.3
	Ga65 – P64 –	104.1	105.6	106.4

	C3			
9	C24 – Ga63 – P62	89.3	90.3	87.9
	Ga63 – P62 – C3	105.8	106.4	107.4

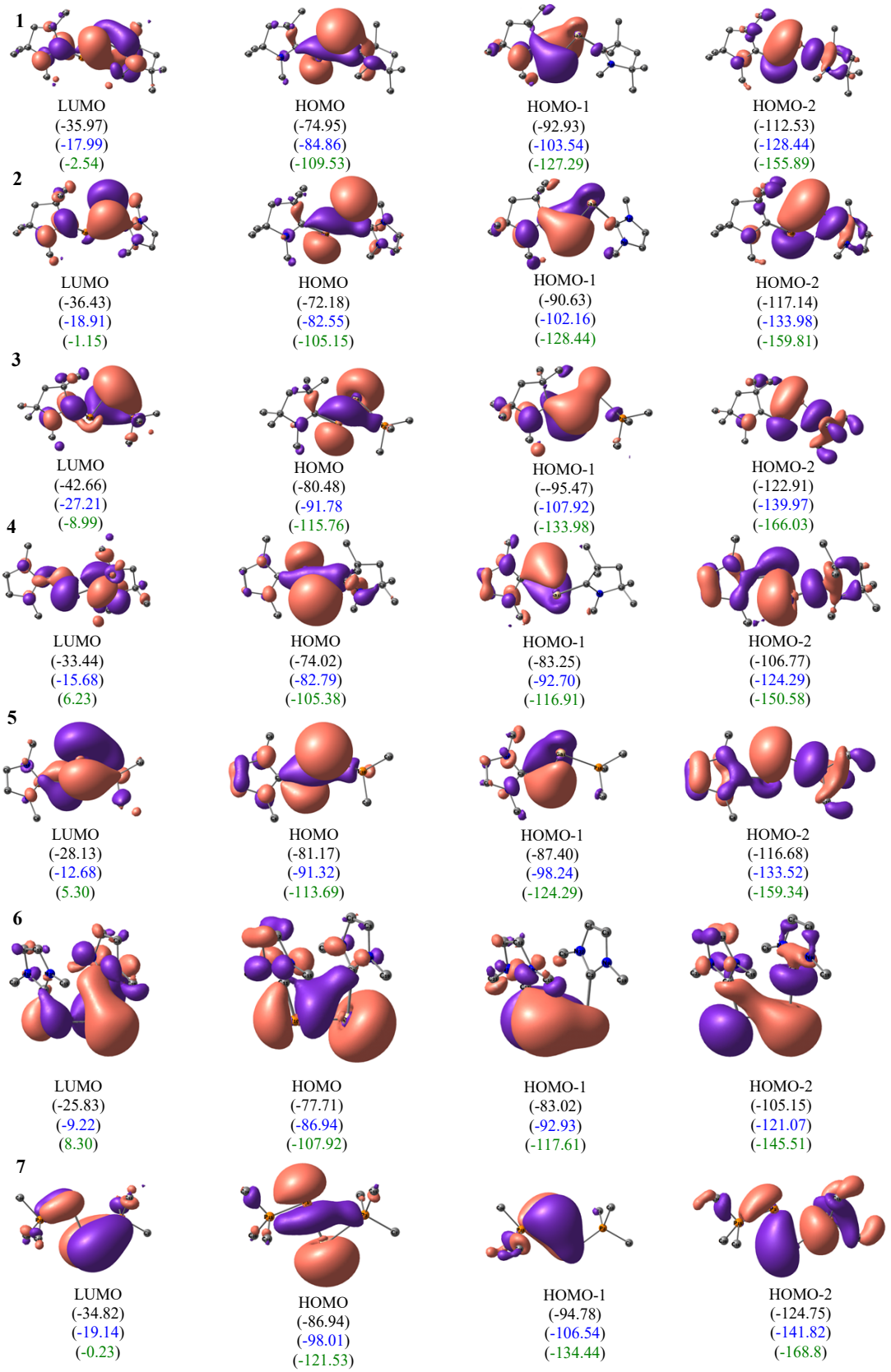

Figure S2. The LUMO, HOMO, HOMO-1 and HOMO-2 of cAAC–P–Ga–cAAC^{Me} (**1**), cAAC–P–Ga–NHC^{Me} (**2**), cAAC–P–Ga–PMe_3 (**3**), NHC^{Me}–P–Ga–cAAC^{Me} (**4**), NHC^{Me}–P–Ga–PMe_3 (**5**), NHC^{Me}–P–Ga–NHC^{Me} (**6**) and PMe_3–P–Ga–PMe_3 (**7**) at BP86-D3(BJ)/def2-

TZVPP (black), B3LYP/def2-TZVPP (blue) and M06-2X/def2-TZVPP (green) levels. Energies of the orbitals are in kcal/mol.

Optimisations of the complexes 8-10

Optimisation of $(cAAC)_2GaP$-CO (10):

We optimised the $(cAAC)_2GaP$-CO (**10**) in singlet ground state at BP86-D3(BJ)/def2-TZVPP level of theory. There is no change of bond length observed for C_{cAAC}–P (1.756 Å) and slight elongation for Ga–C_{cAAC} (2.106 Å) and P – Ga bond (2.416 Å). There is increase of bond angle observed at the P centre (106.2 °) and whereas, Ga centre bond angle decreased from 90.2° to 84.1°. The distance between observed for P and CO, 3.130 Å, is too long to form P–C bond.

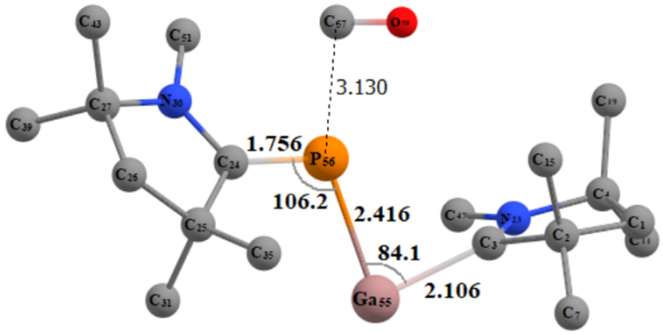

Figure S3. Optimized geometries of compound **10** ($(cAAC)_2GaP$-CO) in singlet ground state at BP86-D3(BJ)/def2-TZVPP level of theory.

Optimisation of $(cAAC)_2GaP$-$Fe(CO)_4$ (8)

The greater dissociation energy and significantly smaller HOMO-LUMO gap of **1** motivated us to investigate the reactivity of **1** as a ligand towards metal carbonyls. In the light of that we optimized the $(cAAC)_2GaP$-$Fe(CO)_4$ (**8**) in singlet ground state at BP86-D3(BJ)/def2-TZVPP level of theory. The dissociation energy calculated for **8** is $[(cAAC)_2GaP\text{-}Fe(CO)_4] \rightarrow (cAAC)_2GaP + [Fe(CO)_4]$ 61.4 kcal/mol and HOMO-LUMO gap is 1.75 eV. There is elongation of bond length observed for C_{cAAC}–P (1.770 Å) and Ga–C_{cAAC} (2.113 Å) bonds and shortening of bond length for P–Ga bond (2.381 Å). There is reduction of bond angle observed at the P centre whereas, at Ga centre bond angle increased from 90.2° to 93.7°. The bond length observed for P and Fe is 2.350 Å which is very similar to the experimentally isolated NHC-phosphindene adduct of $Fe(CO)_4$ (2.399 Å).[6]

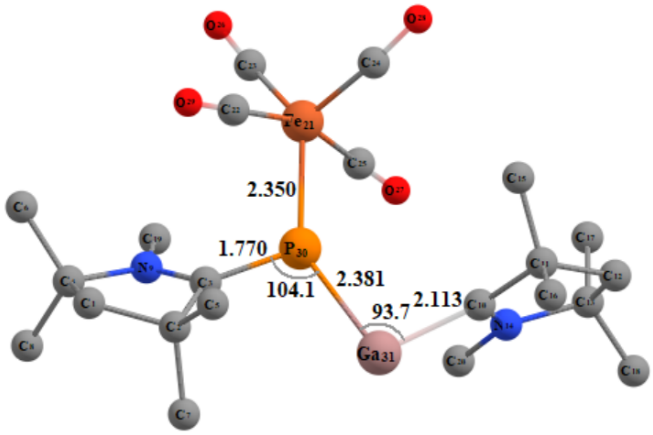

Figure S4. Optimized geometries of compound **8** in singlet ground state at BP86-D3(BJ)/def2-TZVPP level of theory.

$(cAAC)_2GaP\text{-}Ni(CO)_3$ (9)

The greater dissociation energy and significantly smaller HOMO-LUMO gap of **1** motivated us to investigate the reactivity of **1** as a ligand towards metal carbonyls. In the light of that we optimized the $(cAAC)_2GaP\text{-}Ni(CO)_3$ (**9**) in singlet ground state at BP86-D3(BJ)/def2-TZVPP level of theory. The dissociation energy calculated for **9** is $[(cAAC)_2GaP\text{-}Ni(CO)_3] \rightarrow (cAAC)_2GaP + [Ni(CO)_3]$ 39.79 kcal/mol and HOMO-LUMO gap is 1.76 eV. There is no significant change in the bond length of C_{cAAC}–P (1.758 Å) and P–Ga (2.398), whereas, there is notable elongation of Ga–C_{cAAC} (2.135 Å) bonds.There is no change of bond angle observed at the P centre whereas, at Ga centre bond angle reduction from 90.2° to 89.3°. The bond length observed for P and Ni is 2.330 Å which is slightly longer than $Ni(CO)_3(PMe_2Ar^{Dipp2})$ (2.294 Å).[7]

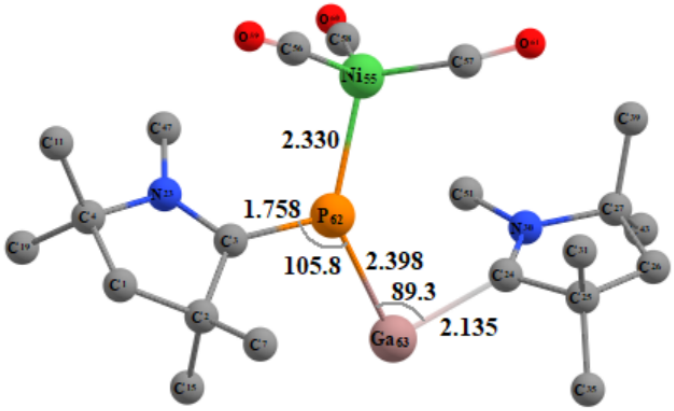

Figure S5. Optimized geometries of compounds **9** in singlet ground state at BP86-D3(BJ)/def2-TZVPP level of theory.

NBO analysis[3] was performed at BP86-D3(BJ)/def2-TZVPP[4] to gain more insight of the electronic structure of **9**. HOMO indicates the presence of lone pair on the Ga centre. HOMO-1 is primarily the π bond at C_{cAAC}–P bond which is slightly extended to the Ga centre. P has natural charge very close to zero (-0.02) and whereas, Ni has a higher negative charge of -1.09 which shows the accepting nature of Ni centre. WBI of C_{cAAC}–P bond is 1.35 indicating the partial double bond nature of the bond and for P – Fe is 0.63 which corresponds to a single bond. As observed in **1**, here also we observe two bonding occupancies for C_{cAAC}–P bond, the first corresponds to the donation from C_{cAAC} to the empty p orbital of P, while the second corresponds to the π-backdonation from P to C_{cAAC}. Notable difference observed from the parent molecule (**1**) is the absence of the lone pair on P.

NBO analyses of complexes 8-9

Table S7. NBO results of the compound $(cAAC)_2GaP{-}Fe(CO)_4$ (**8**) at the BP86-D3(BJ)/def2-TZVPP level of theory. Occupation number (ON), polarization and hybridization of the C_{cAAC}–P, P–Ga, P-Fe and Ga–C_{cAAC} bonds.

	Bond	ON	Polarization and hybridization (%)		WBI	q	
						P	Ga
Compound 8	C3-P64	1.96	P: 34.9	C: 65.1	1.29		
			s(25.19), p(74.32)	s(38.43), p(61.25)			
	Fe55 – P64	1.82	P: 66.2	C: 33.8	0.64	0.13	0.44
		2	s(0.1), p(99.6)	s(0.0), p(99.8)			
		1.74	Fe: 32.7	P: 67.3			
			s(15.86), p(57.71)	s(45.59), p(54.33)			
	P64 – Ga65	1.82	P: 82.6	Ga: 17.4	0.73		
		2	s(29.17), p(70.61)	s(8.62), p(90.98)			
	Ga65 – C24	1.90	C: 86.4	Ga: 13.6	0.58		
			s(37.56), p(62.38)	s(7.88), p(91.75)			

NBO analysis was performed at BP86-D3(BJ)/def2-TZVPP to gain more insight of the electronic structure of **8**. The HOMO of **8** features the lone pair on the Ga atom and also π bond at C_{cAAC}–P bond which is extended to the metal carbonyl and C_{cAAC} (L′). HOMO-1 is the

delocalization of electron density between the carbene carbons and the filled orbitals of the metal carbonyl. HOMO-2 features the electron delocalization from Ga to the C of metal carbonyl. The NBO studies indicate that the P carries a positive charge (0.13), meanwhile Fe carries a negative charge (-2.17), indicating that metal carbonyl an acceptor. WBI of C_{cAAC}–P bond is 1.29 indicating the partial double bond nature of the bond and for P–Fe is 0.64 which corresponds to a single bond. As observed in **1**, here also we observe two bonding occupancies for C_{cAAC}–P bond, the first corresponds to the donation from C_{cAAC} to the empty p orbital of P, while the second corresponds to the π-backdonation from P to C_{cAAC}.

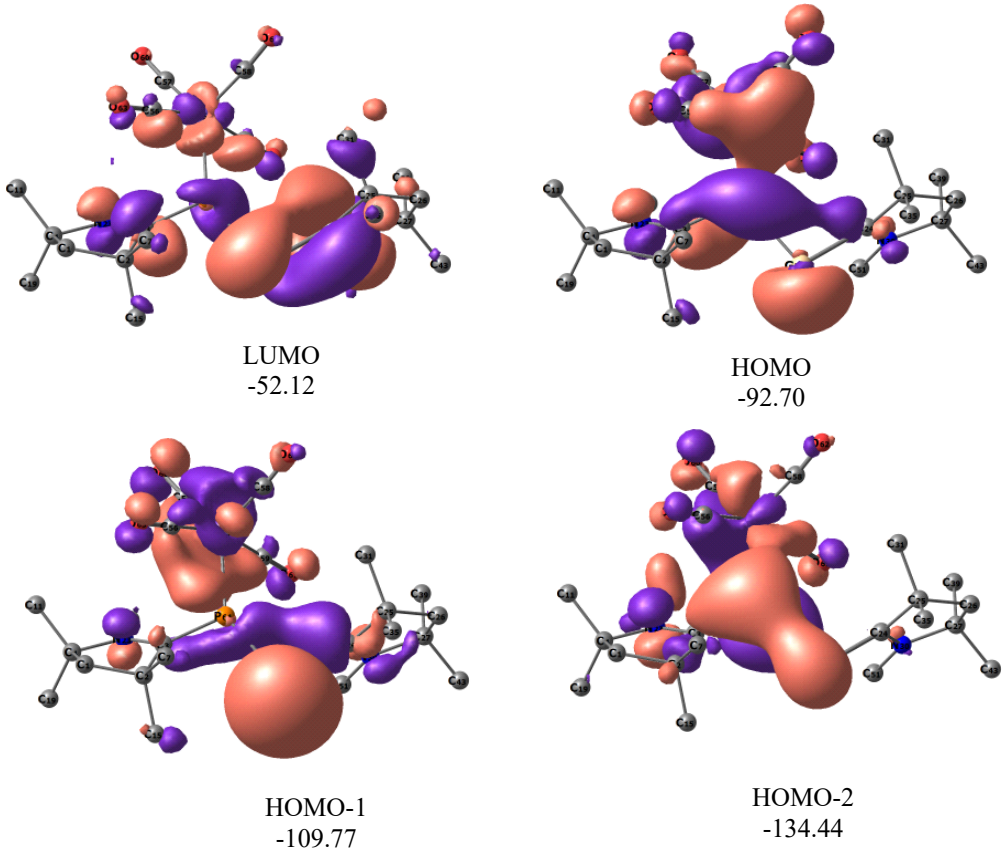

Figure S6. The LUMO, HOMO, HOMO-1 and HOMO-2 of **8** at BP86-D3(BJ)/def2-TZVPP level. Energies are in kcal/mol.

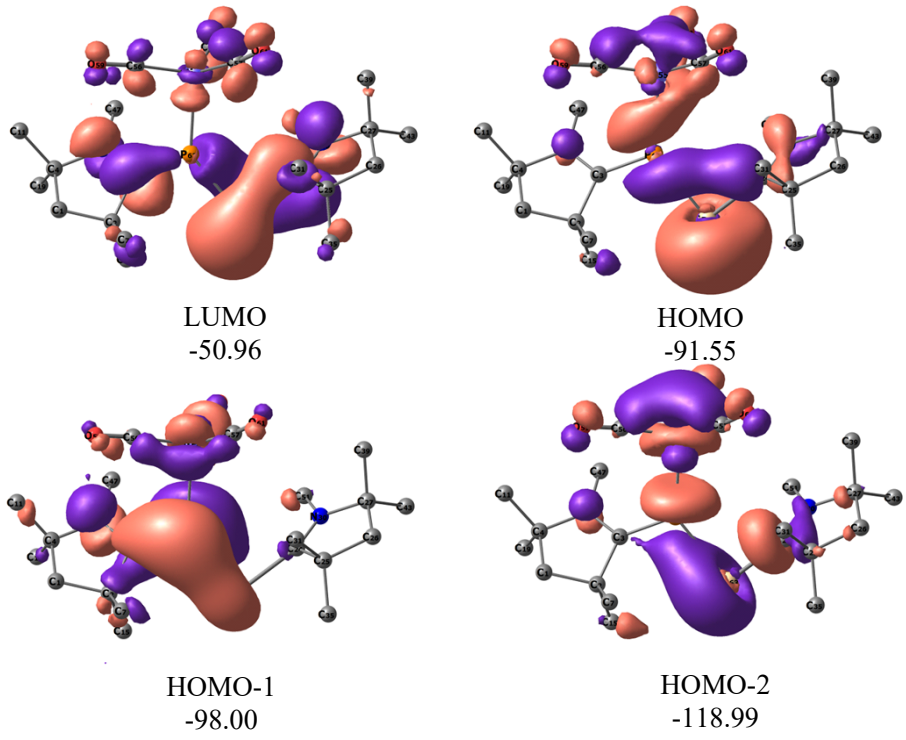

Figure S7. The LUMO, HOMO, HOMO-1 and HOMO-2 of **9** at BP86-D3(BJ)/def2-TZVPP level. Energies are in kcal/mol.

Table S8. NBO results of the compound $(cAAC)_2GaP{-}Ni(CO)_3$ (**9**) at the BP86-D3(BJ)/def2-TZVPP level of theory. Occupation number (ON), polarization and hybridization of the C_{cAAC}–P, P–Ga, P-Ni and Ga–C_{cAAC} bonds.

	Bond	ON	Polarization and hybridization (%)		WBI	q	
						P	Ga
Compound 9	C3-P62	1.97	P: 34.7	C: 65.3	1.35	-0.02	0.408
			s(25.17), p(74.33)	s(38.78), p(60.9)			
	Ni55 – P62	1.85	P: 64.6	C: 35.4	0.63		
			s(0.1), p(99.6)	s(0.11), p(99.7)			
		1.81	Fe: 22.4	P: 77.6			
			s(17.60), p(81.21)	s(46.03), p(53.92)			
	P62 – Ga63	1.83	P: 82.3	Ga: 17.7	0.71		
			s(28.84), p(70.94)	s(8.14), p(91.49)			
	Ga63 – C24	1.90	C: 86.9	Ga: 13.1	0.56		
			s(37.74), p(62.20)	s(6.81), p(92.70)			

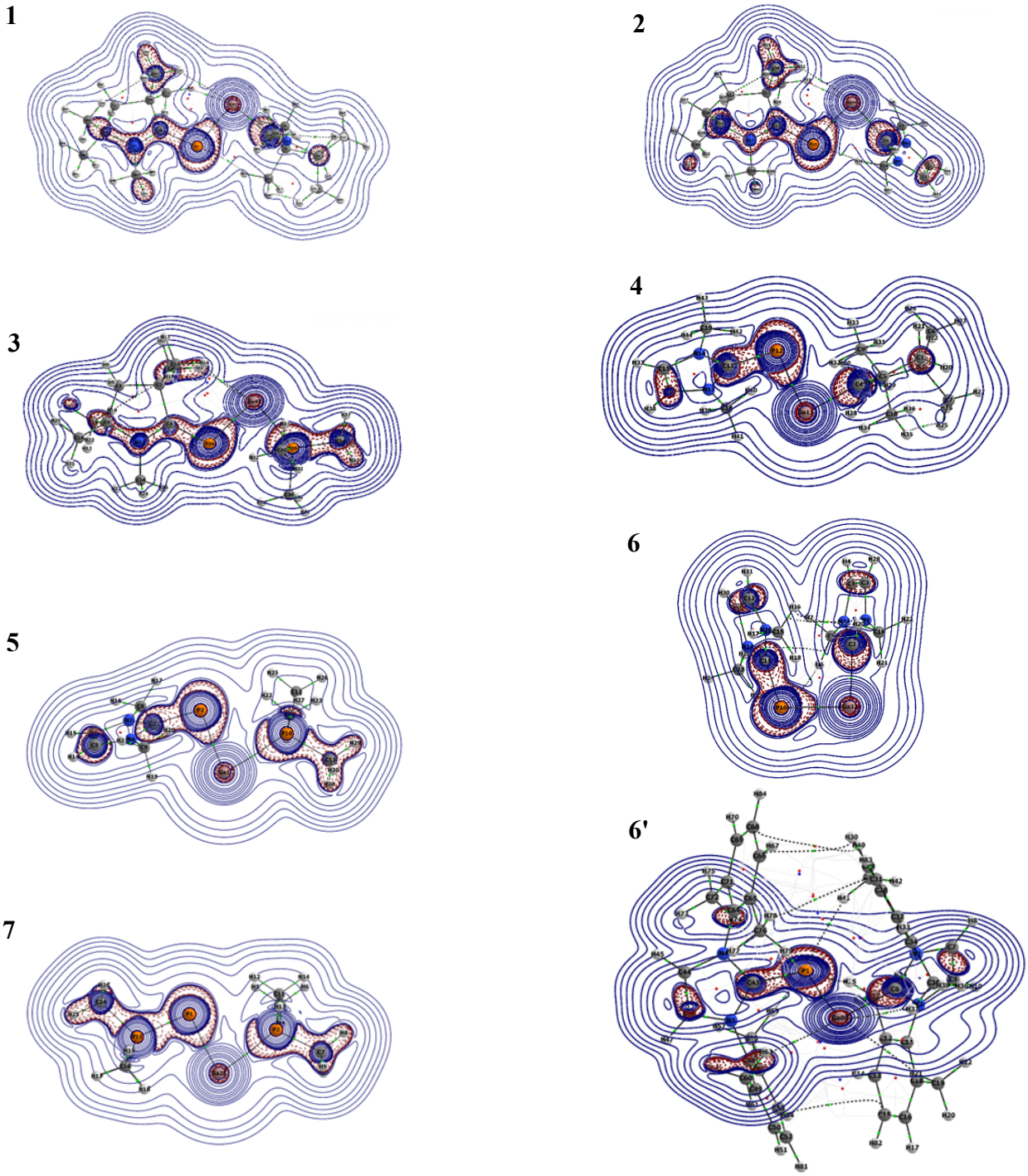

Figure S8. Contour plots of Laplacian distribution [$\nabla^2\rho(r)$] in the P-Ga-L′ plane of compounds **1**-**7**. Solid blue lines indicate the areas of charge concentration ($\nabla^2\rho(r) < 0$) while dotted purple lines denotes charge depletion ($\nabla^2\rho(r) > 0$). Solid lines connecting atomic nuclei (black) are the bond paths.

Table S9. EDA-NOCV results of L–PGa–L′, bonds of L-P-Ga-L′ [L, L′ = $cAAC^{Me}$ (**1**), L = cAAC, L′ = NHC^{Me} (**2**), L = cAAC, L′ = PMe_3 (**3**), L = NHC, L′ = cAAC (**4**), L = NHC, L′ = PMe_3 (**5**), L, L′ = NHC^{Me} (**6**), L, L′ = PMe_3 (**7**)] complexes using four different sets of fragments with different charges and electronic states (S = singlet, D = doublet, T = triplet, Q = quintet) and associated bond types at the BP86-D3(BJ)/TZ2P level. Energies are in kcal/mol. The most favourable fragmentation scheme and bond type is given by the smallest ΔE_{orb} value written in bold.

Molecule	**Bond type**[a]	**Fragments**	ΔE_{int}	ΔE_{Pauli}	ΔE_{elstat}	ΔE_{disp}	ΔE_{orb}
cAAC-P-Ga-cAAC (**1**)	D	$(cAAC)_2$ (S) + P-Ga (S)	-161.1	528.0	-345.1	-19.3	**-324.7**
	E	$(cAAC)_2$ (Q) + P-Ga (Q)	-291.9	424.0	-298.1	-19.3	-398.50
	E (σ, π)	$[(cAAC)_2]^{2+}$ (T) + $[PGa]^{2-}$ (T)	-553.3	611.1	-663.9	-19.3	-481.24
	D+E	$[(cAAC)_2]^{+}$ (D) + $[PGa]^{-}$ (D)	-224.8	520.3	-393.4	-19.3	-332.5
cAAC-P-Ga-NHC (**2**)	D	[(cAAC) (NHC)] (S) + P-Ga (S)	-163.2	545.7	-344.2	-17.5	**-347.2**
	E	[(cAAC) (NHC)] (Q) + P-Ga (Q)	-321.4	348.1	-236.2	-17.5	-415.8
	E (σ, π)	$[(cAAC) (NHC)]^{2+}$ (T) +$[PGa]^{2-}$ (T)	-578.4	671.7	-694.3	-17.5	-538.3
	D+E	$[(cAAC) (NHC)]^{+}$ (D) + $[PGa]^{-}$ (D)	-226.0	546.5	-390.6	-17.5	-364.4
cAAC-P-Ga-PMe_3 (**3**)	D	[(cAAC) (PMe_3)] (S) + P-Ga (S)	-143.30	742.9	-375.3	-17.9	-493.1
	E	[(cAAC) (PMe_3)] (Q) + P-Ga (Q)	-419.8	397.3	-271.4	-17.9	-527.8
	E (σ, π)	$[(cAAC) (PMe_3)]^{2+}$ (T) + $[PGa]^{2-}$ (T)	-567.1	642.1	-655.8	-17.9	-535.5

	D+E	$[(cAAC)(PMe_3)]^+$ (D) + $[PGa]^-$ (D)	-221.2	616.1	-419.3	-17.9	**-400.1**
NHC-P-Ga-cAAC (**4**)	D	[(NHC) (cAAC)] (S) + PGa (S)	-141.4	413.0	-282.6	-18.4	**-252.5**
	E	[(NHC) (cAAC)] (Q) + PGa (Q)	-315.8	351.4	-253.3	-18.4	-395.6
	E (σ, π)	$[(NHC)(cAAC)]^{2+}$ (T) + $[PGa]^{2-}$ (T)	-559.2	489.0	-610.6	-18.4	-419.2
	D+E	$[(NHC)(cAAC)]^+$ (D) + $[PGa]^-$ (D)	-212.2	445.2	-355.2	-18.4	-283.8
NHC-P-Ga-PMe_3 (**5**)	D	$[(NHC)(PMe_3)]$ (S) + P-Ga (S)	-125.6	368.6	-248.5	-16.1	**-229.5**
	E	$[(NHC)(PMe_3)]$ (Q) + P-Ga (Q)	-457.2	341.9	-218.6	-16.1	-564.4
	E (σ, π)	$[(NHC)(PMe_3)]^{2+}$ (T) + $[PGa]^{2-}$ (T)	-573.1	449.8	-599.1	-16.1	-407.7
	D+E	$[(NHC)(PMe_3)]^+$ (D) + $[PGa]^-$ (D)	-293.2	338.5	-299.5	-16.1	-316.2
NHC-P-Ga-NHC (**6**)	D	$[(NHC)_2]$ (S) + PGa (S)	-130.6	448.1	-285.2	-14.1	**-279.3**
	E	$[(NHC)_2]$ (Q) + PGa (Q)	-349.1	363.2	-229.0	-14.1	-469.1
	E (σ, π)	$[(NHC)_2]^{2+}$ (T) + $[PGa]^{2-}$ (T)	-578.7	610.0	-624.1	-14.1	-550.6
	D+E	$[(NHC)_2]^+$ (D) + $[PGa]^-$ (D)	-212.7	517.9	-340.1	-14.1	-376.5
PMe_3-P-Ga- PMe_3 (**7**)	D	$[(PMe_3)_2]$ (S) + PGa (S)	-111.3	493.4	-282.4	-16.6	-305.7
	E	$[(PMe_3)_2]$ (Q) + P-Ga (Q)	-376.3	328.2	-202.3	-16.6	-485.6
	E (σ, π)	$[(PMe_3)2]^{2+}$ (T) +$[PGa]^{2-}$ (T)	-559.2	439.0	-608.9	-16.6	-372.7

	D+E	$[(PMe_3)_2]^+$ (D) +$[PGa]^-$ (D)	-204.3	463.9	-370.1	-16.6	**-281.5**

[a]D = Dative; E = Electronsharing

Table S10. The EDA-NOCV results at the BP86-D3(BJ)/TZ2P level of L–PGa–L′ bonds of L-P-Ga-L′ [L = $cAAC^{Me}$, L′ = PMe_3 (**3**); L, L′ = PMe_3 (**7**)] complexes using [ligands]$^+$ and [P-Ga]$^-$ in the electronic doublet (D) states as interacting fragments. Energies are in kcal/mol.

Energy	**Interaction**	**[(cAAC) (PMe_3)] (D) + [P-Ga] (D)**	**[(PMe_3) (PMe_3)] (D) + [P-Ga] (D)**
Species		**3**	**7**
ΔE_{int}		-221.2	-163.2
ΔE_{Pauli}		616.1	545.7
ΔE_{disp}[a]		-17.9 (2.1%)	-17.5 (2.5%)
ΔE_{elstat}[a]		-419.3 (50.0%)	-344.2 (48.6%)
ΔE_{orb}[a]		-400.1 (47.8%)	-347.2 (48.9%)
$\Delta E_{orb(1)}$[b]	L P-Ga L′ σ electron sharing	-269.4 (67.3%)	-185.9 (66.0%)
$\Delta E_{orb(2)}$[b]	L→P-Ga←L′ σ donation	-54.6 (13.6%)	-43.1 (15.3%)
$\Delta E_{orb(3)}$[b]	L←P-Ga→L′ π backdonation	-41.2 (10.3%)	-18.8 (6.7%)
$\Delta E_{orb(rest)}$		-34.8 (8.7%)	-33.7 (12%)

cAAC-PGa-NHC	[(cAAC) (NHC)] (S)	[P-Ga] (S)
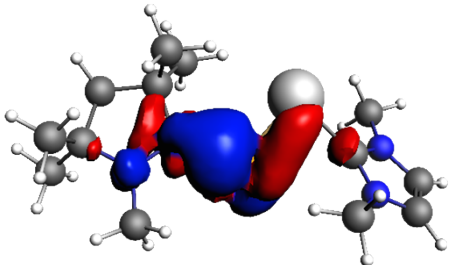	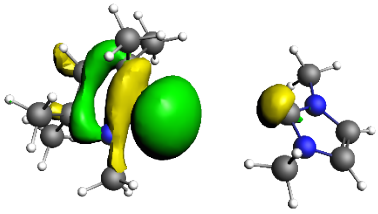	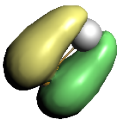
$\Delta\rho_{(1)}$	HOMO (ε = -89.93)	LUMO (ε = -111.61)
$\Delta E_{orb(1)}$ = -214.1; $\lvert\nu_{1\alpha}/\nu_{1\beta}\rvert$ = 0.71/0.71		
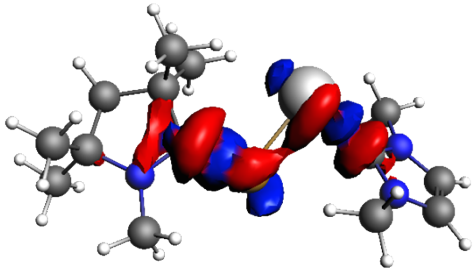	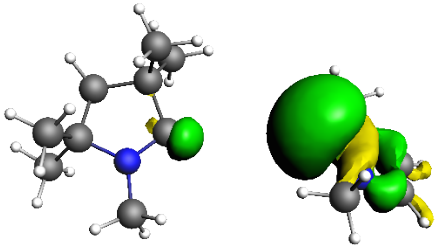	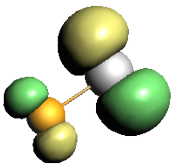
$\Delta\rho_{(2)}$	HOMO-1 (ε = -99.62)	LUMO+1 (ε = -50.50)
$\Delta E_{orb(2)}$ = -69.4; $\lvert\nu_{2\alpha}/\nu_{2\beta}\rvert$ = 0.36/0.36		
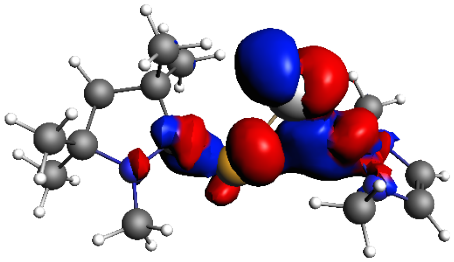	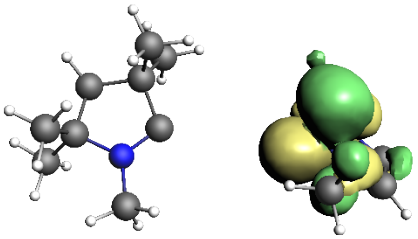	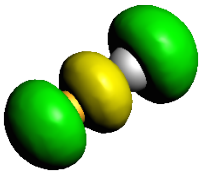
$\Delta\rho_{(3)}$	LUMO+3 (ε = 3.23)	HOMO (ε = -106.54)
$\Delta E_{orb(3)}$ = -27.4; $\lvert\nu_{3\alpha}/\nu_{3\beta}\rvert$ = 0.28/0.28		
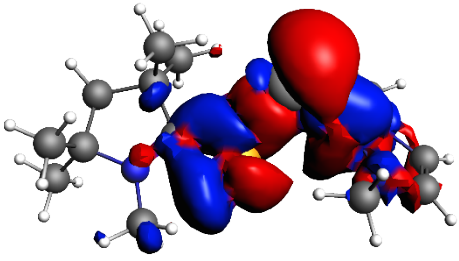	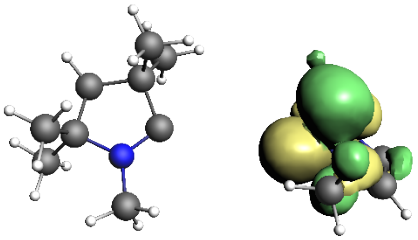	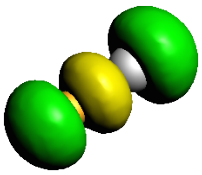
$\Delta\rho_{(4)}$	LUMO+3 (ε = 3.23)	HOMO (ε = -106.54)
$\Delta E_{orb(4)}$ = -15.2.; $\lvert\nu_{4\alpha}/\nu_{4\beta}\rvert$ = 0.20/0.20		

Figure S9. The shape of the deformation densities $\Delta\rho_{(1)-(4)}$ that correspond to $\Delta E_{orb(1)-(4)}$, and the associated MOs of cAAC-P-Ga-NHC (**2**) and the fragments orbitals of [(cAAC) (NHC)] and [P-Ga] in the Singlet state (S) at the BP86-D3(BJ)/TZ2P level. Isosurface values are 0.003 au for $\Delta\rho_{(1)}$ and 0.002

au for $\Delta\rho_{(2\text{-}4)}$. The eigenvalues $|\nu_n|$ give the size of the charge migration in e. The direction of the charge flow of the deformation densities is red→blue. Energy values are in kcal/mol.

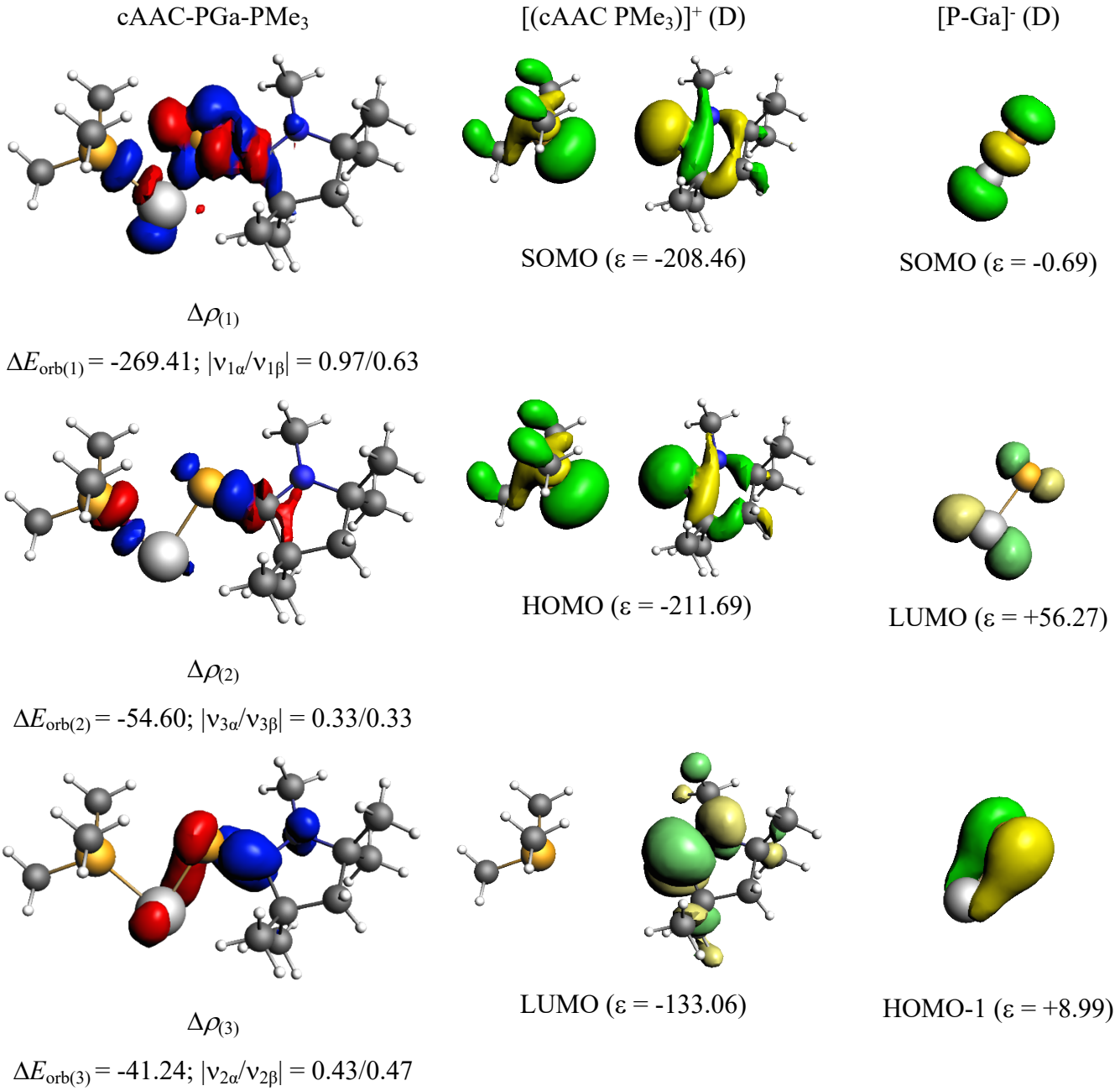

Figure S10. The shape of the deformation densities $\Delta\rho_{(1)\text{-}(3)}$ that correspond to $\Delta E_{orb(1)\text{-}(3)}$, and the associated MOs of cAAC-P-Ga-PMe_3 (**3**) and the fragments orbitals of $[(cAAC)(PMe_3)]^+$ and $[P\text{-}Ga]^-$ in the doublet state (D) at the BP86-D3(BJ)/TZ2P level. Isosurface values are 0.003 au for $\Delta\rho_{(1\text{-}3)}$. The eigenvalues $|\nu_n|$ give the size of the charge migration in e. The direction of the charge flow of the deformation densities is red→blue. Energy values are in kcal/mol.

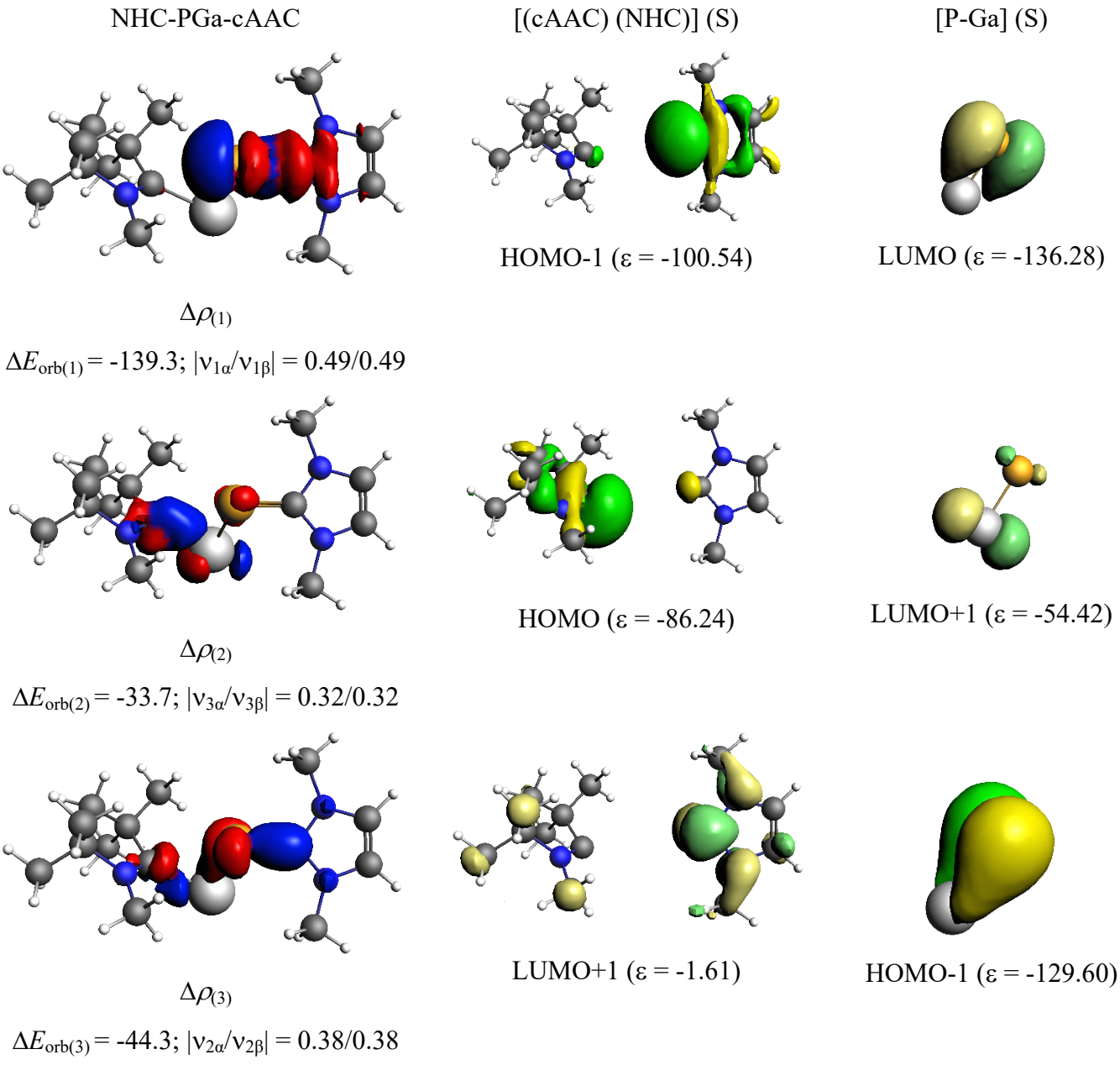

Figure S11. The shape of the deformation densities $\Delta\rho_{(1)-(4)}$ that correspond to $\Delta E_{orb(1)-(4)}$, and the associated MOs of NHC-P-Ga-cAAC (**4**) and the fragments orbitals of [(NHC) (cAAC)] and [P-Ga] in the Singlet state (S) at the BP86-D3(BJ)/TZ2P level. Isosurface values are 0.003 au for $\Delta\rho_{(1)}$ and 0.001 au for $\Delta\rho_{(2-3)}$. The eigenvalues $|\nu_n|$ give the size of the charge migration in e. The direction of the charge flow of the deformation densities is red→blue. Energy values are in kcal/mol.

NHC-PGa-NHC	[$(NHC)_2$] (S)	[P-Ga] (S)
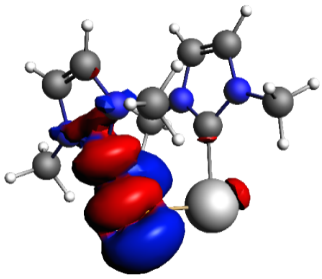	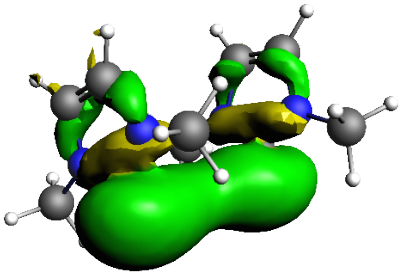	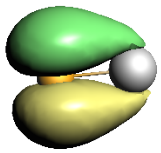
$\Delta\rho_{(1)}$	HOMO-1 (ε = -109.53)	LUMO (ε = -136.74)
$\Delta E_{orb(1)}$ = -158.7; $\lvert\nu_{1\alpha}/\nu_{1\beta}\rvert$ = 0.61/0.61		
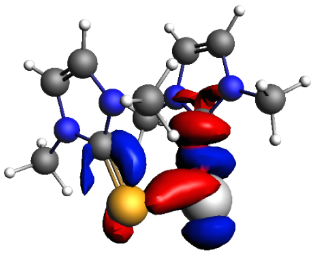	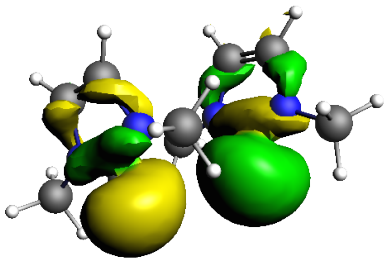	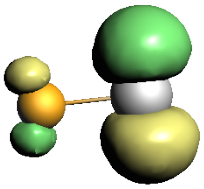
$\Delta\rho_{(2)}$	HOMO (ε = -95.93)	LUMO+1 (ε = -54.19)
$\Delta E_{orb(2)}$ = -31.8; $\lvert\nu_{2\alpha}/\nu_{2\beta}\rvert$ = 0.29/0.29		
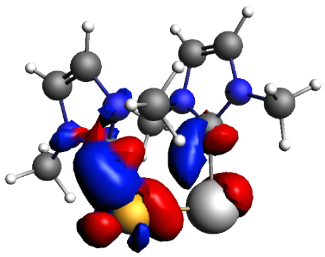	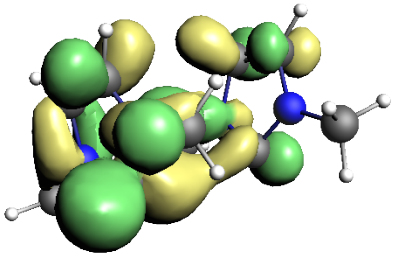	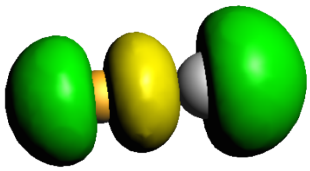
$\Delta\rho_{(3)}$	LUMO+2 (ε = -3.46)	HOMO (ε = -117.61)
$\Delta E_{orb(3)}$ = -50.5; $\lvert\nu_{3\alpha}/\nu_{3\beta}\rvert$ = 0.37/0.37		
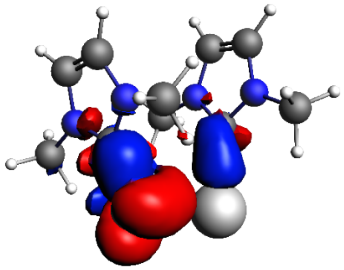	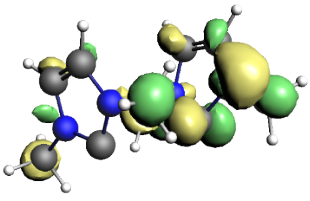	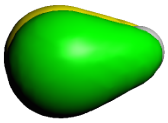
$\Delta\rho_{(4)}$	LUMO +4 (ε = +3.46)	HOMO-1 (ε = -121.76)
$\Delta E_{orb(4)}$ = -21.2; $\lvert\nu_{4\alpha}/\nu_{4\beta}\rvert$ = 0.20/0.20		

Figure S12. The shape of the deformation densities $\Delta\rho_{(1)-(4)}$ that correspond to $\Delta E_{orb(1)-(4)}$, and the associated MOs of NHC-P-Ga-NHC (**6**) and the fragments orbitals of $[(NHC)_2]$ and [P-Ga] in the Singlet state (S) at the BP86-D3(BJ)/TZ2P level. Isosurface values are 0.003 au for $\Delta\rho_{(1)}$, 0.002 au for $\Delta\rho_{(2-3)}$ and 0.001 au for $\Delta\rho_{(4)}$. The eigenvalues $|\nu_n|$ give the size of the charge migration in e. The direction of the charge flow of the deformation densities is red→blue. Energy values are in kcal/mol.

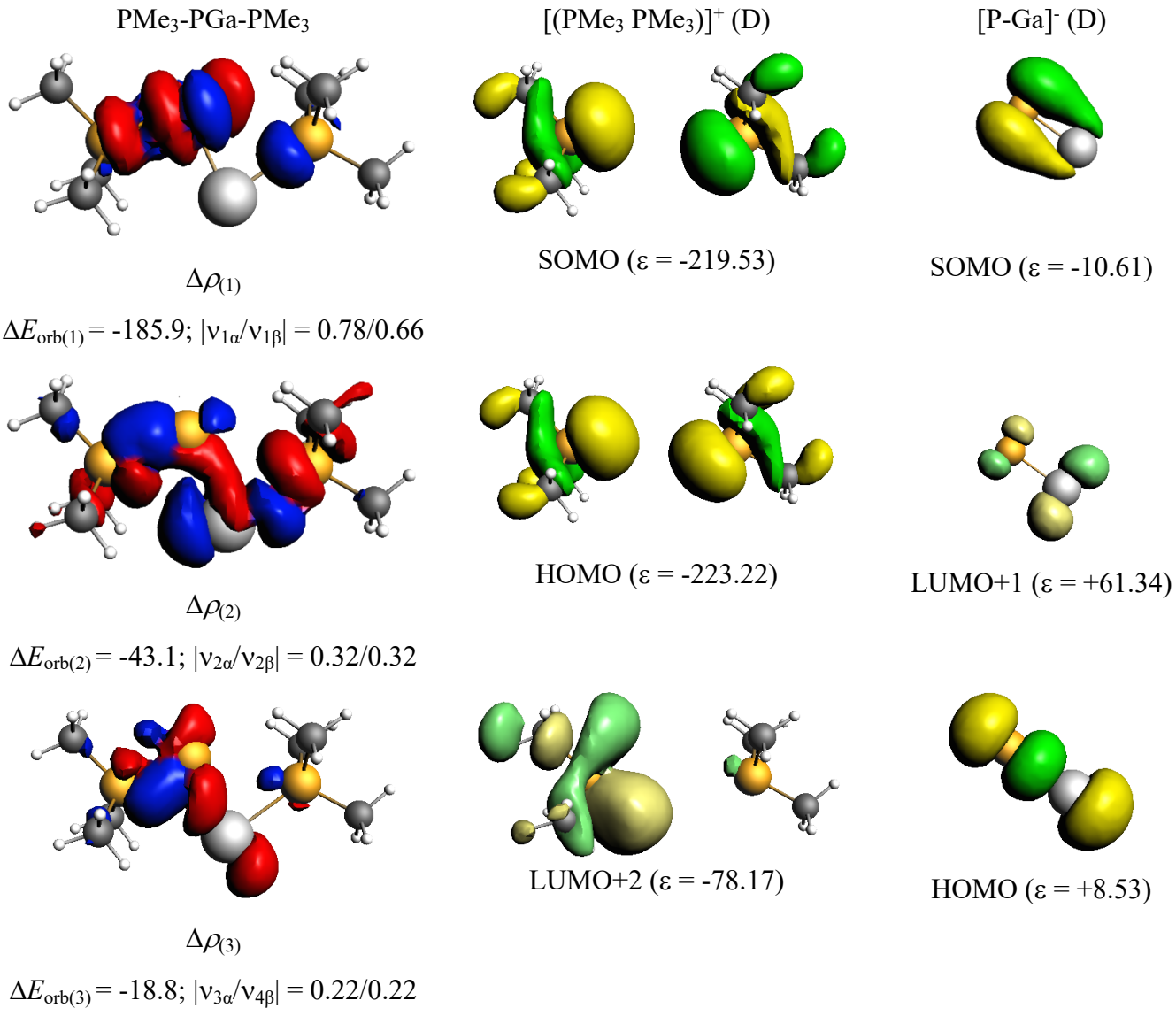

Figure S13. The shape of the deformation densities $\Delta\rho_{(1)-(3)}$ that correspond to $\Delta E_{orb(1)-(3)}$, and the associated MOs of PMe_3-P-Ga-PMe_3 (**7**) and the fragments orbitals of $[(PMe_3)\ (PMe_3)]^+$ and $[P\text{-}Ga]^-$ in the doublet state (D) at the BP86-D3(BJ)/TZ2P level. Isosurface values are 0.003 au for $\Delta\rho_{(1)}$ and 0.001 au for $\Delta\rho_{(2-3)}$. The eigenvalues $|\nu_n|$ give the size of the charge migration in e. The direction of the charge flow of the deformation densities is red→blue. Energy values are in kcal/mol.

Table S11. The EDA-NOCV results at the M06-2X/TZ2P level of L–PGa–L′ bonds of L-P-Ga-L′ complex [L, L′ = $cAAC^{Me}$ (**1**), L = $cAAC^{Me}$, L′ = NHC^{Me} (**2**), L = NHC^{Me}, L′ = $cAAC^{Me}$ (**4**), L, L′ = PMe_3 (**7**)] using [ligands] and [P-Ga] in the electronic singlet (S) states as interacting fragments. Energies are in kcal/mol.

Energy	**Interaction**	**[(cAAC)$_2$] (S) + [P-Ga] (S)**	**[(cAAC) (NHC)] (S) + [P-Ga] (S)**	**[(NHC) (cAAC)] (S) + [P-Ga] (S)**	**[(PMe_3)$_2$] (S) + [P-Ga] (S)**
species		**1**	**2**	**4**	**7**
ΔE_{int}		-140.1	-136.3	-125.3	-96.9
ΔE_{Pauli}		553.9	508.3	401.1	291.3
ΔE_{disp}[a]		-0.38 (0.1%)	-0.27 (0.04%)	-0.3 (0.05%)	-0.14 (0.03%)
ΔE_{elstat}[a]		-360.5 (52%)	-331.3 (51.4%)	-292.1 (55.5%)	-195.7 (50.4%)
ΔE_{orb}[a]		-333.1 (48%)	-312.9 (48.5%)	-234.0 (44.45%)	-192.4 (49.6%)
$\Delta E_{orb(1)}$[b]	L→P-Ga←L′ σ donation	-215.5 (64.7%)	-203.6 (65.1%)	-134.1 (57.3%)	-126.8 (65.9%)
$\Delta E_{orb(2)}$[b]	L→P-Ga←L′ σ donation	-37.6 (11.3%)	-28.5 (9.1%)	-44.0 (18.8%)	29.3 (15.3%)
$\Delta E_{orb(3)}$[b]	L←P-Ga→L′ π backdonation	-49.6 (14.9%)	-53.4 (17.1%)	-27.7 (11.8%)	18.8 (9.8%)
$\Delta E_{orb(4)}$[b]	L←P-Ga→L′ π backdonation	-16.3 (4.9%)		-14.1 (6.0%)	13.1 (6.8%)
$\Delta E_{orb(rest)}$		-14.1 (4.2%)	-27.4 (8.7%)	-14.1 (6.0%)	4.4 (2.2%)

Table S12. EDA-NOCV results of (L)P–Ga(L′) bond of L-P-Ga-L′ [L, L′ = $cAAC^{Me}$ (**1**), L = cAAC, L′ = NHC^{Me} (**2**), L = cAAC, L′ = PMe_3 (**3**), L = NHC, L′ = cAAC (**4**), L = NHC, L′ = PMe_3 (**5**), L, L′ = NHC^{Me} (**6**), L, L′ = PMe_3 (**7**)] complexes using three different sets of fragments with different charges and electronic states (S = singlet, D = doublet) and associated bond types at the BP86-D3(BJ)/TZ2P level. Energies are in kcal/mol. The most favourable fragmentation scheme and bond type is given by the smallest ΔE_{orb} value written in bold.

Molecule	**Bond type**[a]	**Fragments**	ΔE_{int}	ΔE_{Pauli}	ΔE_{elstat}	ΔE_{disp}	ΔE_{orb}
cAAC-P-Ga-cAAC (**1**)	E	cAAC-P (D) + Ga-cAAC (D)	-50.8	154.6	-99.6	-8.7	**97.1**
	D	$[cAAC\text{-}P]^-$ (S) + $[Ga\text{-}cAAC]^+$ (S)	-153.6	183.0	-206.2	-8.7	-121.7
	D	$[cAAC\text{-}P]^+$ (S) +	-227.3	227.9	-216.9	-8.7	-229.5

		[Ga-cAAC]$^-$ (S)					
cAAC-P-Ga-NHC (**2**)	E	cAAC-P (D) + Ga -NHC (D)	-56.2	166.6	-108.5	-8.3	**-106.0**
	D	[cAAC-P]$^-$ (S) + [Ga -NHC]$^+$ (S)	-146.4	173.0	-199.0	-8.3	-112.1
	D	[cAAC-P]$^+$ (S) + [Ga-NHC]$^-$ (S)	-321.0	242.8	-243.1	-8.3	-312.3
cAAC-P-Ga-PMe_3 (**3**)	E	cAAC-P (D) + Ga-PMe_3 (D)	-60.9	180.3	-114.3	-9.3	-117.6
	D	[cAAC-P]$^-$ (S) + [Ga -PMe_3]$^+$ (S)	-159.8	172.6	-208.4	-9.3	**-114.7**
	D	[cAAC-P]$^+$ (S) + [Ga -PMe_3]$^-$ (S)	-253.5	287.0	-246.9	-9.3	-284.3
NHC-P-Ga-cAAC (**4**)	E	cAAC-P (D) + Ga-(N^iPr_2)$_2$ (D)	-62.5	177.1	-117.1	-9.4	-113.1
	D	[cAAC-P]$^-$ (S) + [Ga-(N^iPr_2)$_2$]$^+$ (S)	-159.9	163.6	-197.6	-9.4	**-110.6**
	D	[cAAC-P]$^+$ (S) + [Ga-(N^iPr_2)$_2$]$^-$ (S)	-224.0	273.7	-239.4	-9.4	-248.9
NHC-P−Ga-PMe_3 (**5**)	E	NHC-P (D) + Ga-NHC (D)	-72.9	180.9	123.5	-8.5	-121.8
	D	[NHC-P]$^-$ (S) + [Ga-NHC]$^+$ (S)	-165.1	150.2	-194.2	-8.5	**-112.6**
	D	[NHC-P]$^+$ (S) + [Ga-NHC]$^-$ (S)	-247.1	244.8	-221.6	-8.5	-261.8
NHC-P−Ga-NHC (**6**)	E	PMe3-P (D) + Ga - PMe3 (D)	-62.9	174.3	-108.0	-14.9	-114.4
	D	[PMe3-P]$^-$ (S) + [Ga-PMe3]$^+$ (S)	-148.2	145.1	-177.2	-14.9	**-101.2**
	D	[PMe3-P]$^+$ (S) + [Ga- PMe3]$^-$ (S)	-359.9	314.2	-286.7	-14.9	-372.5

PMe_3-P−Ga-PMe_3 (**7**)	E	PMe3-P (D) + Ga - PMe3 (D)	-75.3	156.5	-107.7	-9.0	-115.1
	D	$[PMe3-P]^-$ (S) + $[Ga-PMe3]^+$ (S)	-163.3	167.6	-207.0	-9.0	**-114.9**
	D	$[PMe3-P]^+$ (S) + $[Ga- PMe3]^-$ (S)	-305.0	237.8	-222.8	-9.0	-311.1

Table S13. The EDA-NOCV results of P−Ga bond of compounds **1** and **2** at the BP86-D3(BJ)/TZ2P level. Energies are in kcal/mol.

Energy	**Interaction**	**cAAC-P (D) + Ga-cAAC (D)**	**cAAC-P (D) + Ga-NHC (D)**
ΔE_{int}		-50.8	-56.2
ΔE_{Pauli}		154.6	166.6
ΔE_{disp}[a]		-8.7 (4.3%)	-8.3
ΔE_{elstat}[a]		-99.6 (48.4%)	-108.5 (48.7%)
ΔE_{orb}[a]		-97.1 (47.3%)	-106.0 (47.6%)
$\Delta E_{orb(1)}$[b]	LP–GaL′ σ e^- sharing	-77.3 (79.6%)	-86.1 (81.3%)
$\Delta E_{orb(2)}$[b]	LP→GaL′ π donation	-7.8 (8.1%)	-8.9 (8.4%)
$\Delta E_{orb(rest)}$[b]		-12.0 (12.3%)	-10.9 (10.3%)

[a]The values in the parentheses show the contribution to the total attractive interaction $\Delta E_{elstat} + \Delta E_{orb} + \Delta E_{disp}$.

[b]The values in parentheses show the contribution to the total orbital interaction ΔE_{orb}.

Table S14. The EDA-NOCV results of P−Ga bond of compounds **3**-**7** at the BP86-D3(BJ)/TZ2P level. Energies are in kcal/mol.

Energy	**Interaction**	**[(cAAC)P]$^-$ (S) + [Ga(PMe$_3$)]$^+$ (S)**	**[(NHC)P]$^-$ (S) + [Ga(cAAC)]$^+$ (S)**	**[(NHC)P]$^-$ (S) + [Ga(PMe$_3$)]$^+$ (S)**	**[(NHC)P]$^-$ (S) + [Ga(NHC)]$^+$ (S)**	**[(PMe$_3$)P]$^-$ (S) + [Ga(PMe$_3$)]$^+$ (S)**
ΔE_{int}		-159.8	-153.9	-165.1	-148.2	-163.3
ΔE_{Pauli}		-208.4	163.6	150.3	145.1	167.6
ΔE_{disp}[a]		-9.3 (2.8%)	-9.4 (3.0%)	-8.5 (2.7%)	-14.9 (5.1%)	-9.0 (2.7%)
ΔE_{elstat}[a]		-208.4 (62.7%)	-197.6 (62.2%)	-194.3 (61.6%)	-177.2 (60.4%)	-207.0 (62.6%)
ΔE_{orb}[a]		-114.7 (34.5%)	-110.6 (34.8%)	-112.6 (35.7%)	-101.2 (34.5%)	-114.9 (34.7%)
$\Delta E_{orb(1)}$[b]	LP–GaL′ σ e$^-$ sharing	-75.5 (68.8%)	-72.7 (65.7%)	-69.8 (62.0%)	-61.0 (60.3%)	-74.8 (65.1%)
$\Delta E_{orb(2)}$[b]	LP→GaL′ π donation	-19.4 (16.9%)	-19.8 (17.9%)	-24.5 (21.8%)	-21.1 (20.8%)	-21.0 (18.3%)
$\Delta E_{orb(rest)}$[b]		-19.8 (17.3%)	-18.1 (16.4%)	-28.8 (25.6%)	-19.1 (18.9%)	-19.1 (16.6%)

[a]The values in the parentheses show the contribution to the total attractive interaction ΔE_{elstat} + ΔE_{orb} + ΔE_{disp}.

[b]The values in parentheses show the contribution to the total orbital interaction ΔE_{orb}.

(cAAC)P-Ga(cAAC) (**1**)	(cAAC)P (D)	Ga(cAAC) (D)
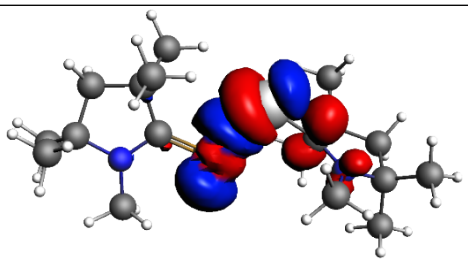 $\Delta\rho_{(1)}$ $\Delta E_{orb(1)}$ = -77.9; $\lvert\nu_{1\alpha}/\nu_{1\beta}\rvert$ = 0.49/0.79	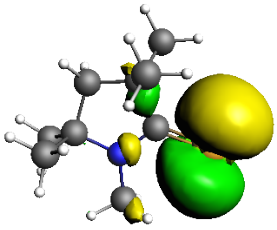 SOMO (ε = -93.62)	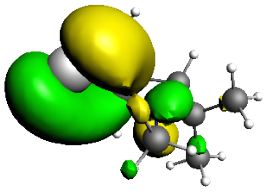 SOMO (ε = -59.26)
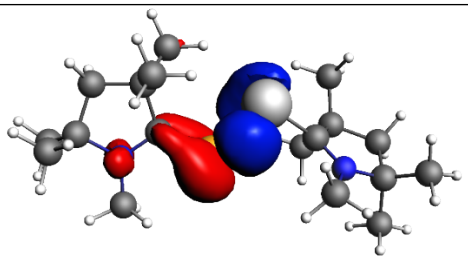 $\Delta\rho_{(2)}$ $\Delta E_{orb(2)}$ = -7.8; $\lvert\nu_{2\alpha}/\nu_{2\beta}\rvert$ = 0.20/0.20	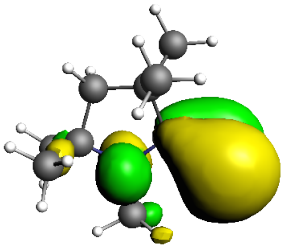 HOMO (ε = -102.62)	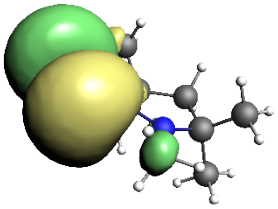 LUMO (ε = -40.82)

Figure S14. The shape of the deformation densities $\Delta\rho_{(1)\text{-}(2)}$ that correspond to $\Delta E_{orb(1)\text{-}(2)}$, and the associated MOs of (cAAC)P-Ga(cAAC) (**1**) and the fragments orbitals of cAAC-P and Ga(cAAC) in the doublet state at the BP86-D3(BJ)/TZ2P level. Isosurface values are 0.002 au for $\Delta\rho_{(1)}$ and isosurface value 0.001 for $\Delta\rho_{(2)}$. The eigenvalues $\lvert\nu_n\rvert$ give the size of the charge migration in e. The direction of the charge flow of the deformation densities is red→blue.

(cAACP)-Ga(NHC) (**2**)	(cAAC)P (D)	Ga(NHC) (D)
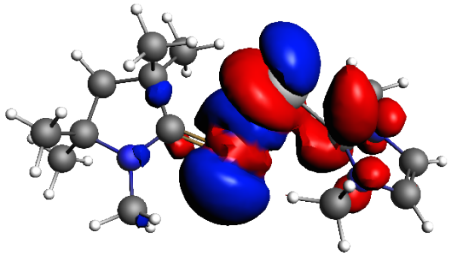 $\Delta\rho_{(1)}$ $\Delta E_{orb(1)}$ = -86.1; $\lvert\nu_{1\alpha}/\nu_{1\beta}\rvert$ = 0.81/0.43	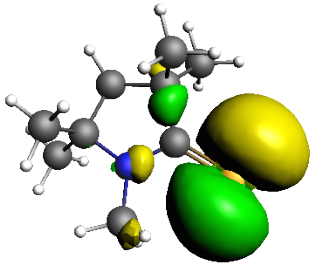 SOMO (ε = -93.85)	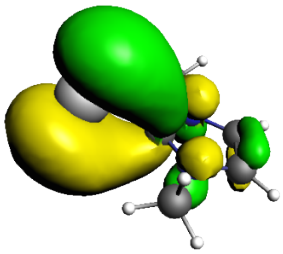 SOMO (ε = -48.66)
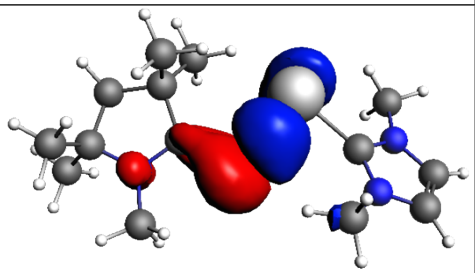 $\Delta\rho_{(2)}$ $\Delta E_{orb(2)}$ = -8.9; $\lvert\nu_{2\alpha}/\nu_{2\beta}\rvert$ = 0.21/0.21	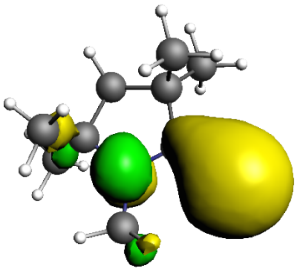 HOMO (ε = -102.62)	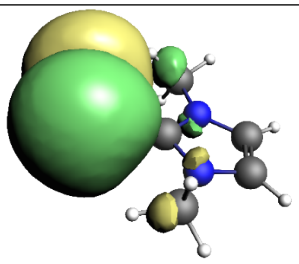 LUMO (ε = -43.12)

Figure S15. The shape of the deformation densities $\Delta\rho_{(1)-(2)}$ that correspond to $\Delta E_{orb(1)-(2)}$, and the associated MOs of (cAAC)P-Ga(NHC) (**2**) and the fragments orbitals of cAAC-P and Ga(NHC) in the doublet state at the BP86-D3(BJ)/TZ2P level. Isosurface values are 0.002 au for $\Delta\rho_{(1)}$ and isosurface value 0.001 for $\Delta\rho_{(2)}$. The eigenvalues $|\nu_n|$ give the size of the charge migration in e. The direction of the charge flow of the deformation densities is red→blue.

(cAAC)P-Ga(PMe_3) (**3**)	[(cAAC)P]$^-$ (S)	[Ga(PMe_3)]$^+$ (D)
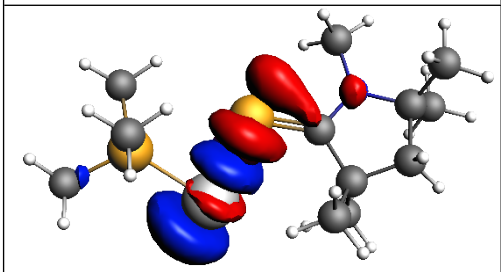 $\Delta\rho_{(1)}$ $\Delta E_{orb(1)}$ = -75.5; $\lvert\nu_{1\alpha}/\nu_{1\beta}\rvert$ = 0.46/0.46	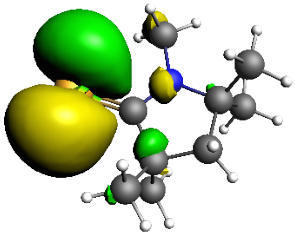 HOMO (ε = 37.36)	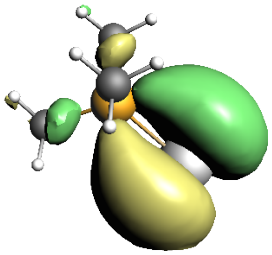 LUMO (ε = -173.41)
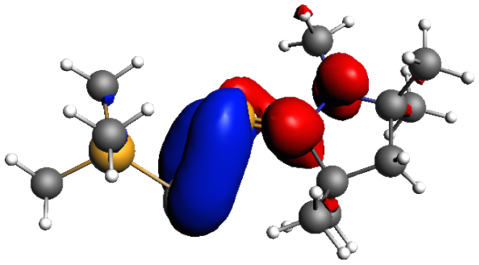 $\Delta\rho_{(2)}$ $\Delta E_{orb(2)}$ = -19.4; $\lvert\nu_{2\alpha}/\nu_{2\beta}\rvert$ = 0.26/0.26	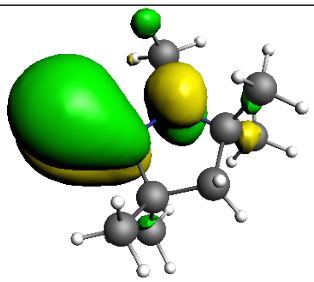 HOMO-1 (ε = 13.84)	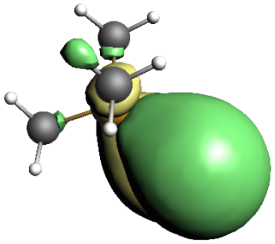 LUMO+1 (ε = -172.95)

Figure S16. The shape of the deformation densities $\Delta\rho_{(1)-(2)}$ that correspond to $\Delta E_{orb(1)-(2)}$, and the associated MOs of (cAAC)P-Ga(PMe_3) (**3**) and the fragments orbitals of [(cAAC)P]$^-$ and [Ga(PMe_3)]$^+$ in the singlet state at the BP86-D3(BJ)/TZ2P level. Isosurface values are 0.003 au for $\Delta\rho_{(1)}$ and isosurface value 0.001 for $\Delta\rho_{(2)}$. The eigenvalues $|\nu_n|$ give the size of the charge migration in e. The direction of the charge flow of the deformation densities is red→blue. Energy values are in kcal/mol.

(NHC)P-Ga(cAAC) (**4**)	$[(NHC)P]^-$ (S)	$[Ga(cAAC)]^+$ (S)
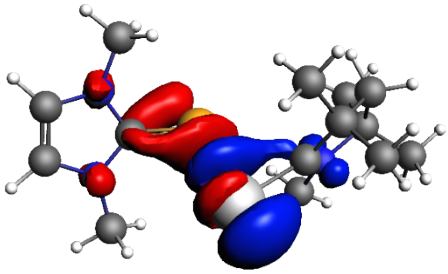 $\Delta\rho_{(1)}$ $\Delta E_{orb(1)}$ = -72.73; $\lvert\nu_{1\alpha}/\nu_{1\beta}\rvert$ = 0.51/0.51	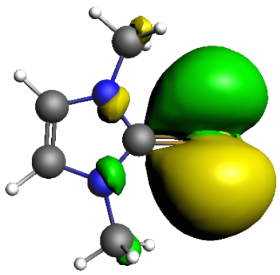 HOMO (ε = 40.82)	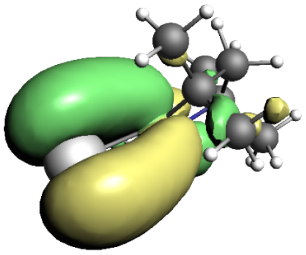 LUMO (ε = -168.57)
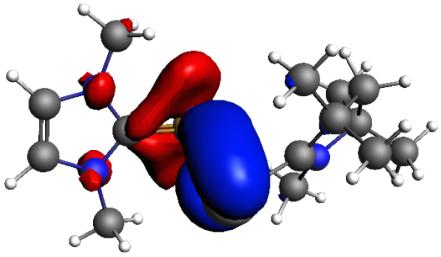 $\Delta\rho_{(2)}$ $\Delta E_{orb(2)}$ = -19.8; $\lvert\nu_{2\alpha}/\nu_{2\beta}\rvert$ = 0.26/0.26	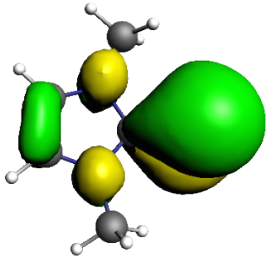 HOMO-1 (ε = 29.74)	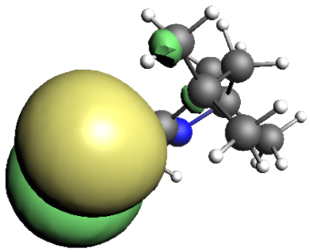 LUMO+1 (ε = -151.04)

Figure S17. The shape of the deformation densities $\Delta\rho_{(1)-(2)}$ that correspond to $\Delta E_{orb(1)-(2)}$, and the associated MOs of (NHC)P-Ga(cAAC) (**4**) and the fragments orbitals of $[(NHC)P]^-$ and $[Ga(cAAC)]^+$ in the singlet state at the BP86-D3(BJ)/TZ2P level. Isosurface values are 0.003 au for $\Delta\rho_{(1)}$ and isosurface value 0.001 for $\Delta\rho_{(2)}$. The eigenvalues $|\nu_n|$ give the size of the charge migration in e. The direction of the charge flow of the deformation densities is red→blue. Energy values are in kcal/mol.

(NHC)P-Ga(PMe_3) (**5**)	$[(NHC)P]^-$ (S)	$[Ga(NHC)]^+$ (S)
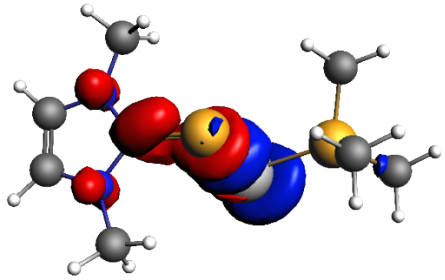 $\Delta\rho_{(1)}$ $\Delta E_{orb(1)}$ = -69.8; $\lvert\nu_{1\alpha}/\nu_{1\beta}\rvert$ = 0.46/0.46	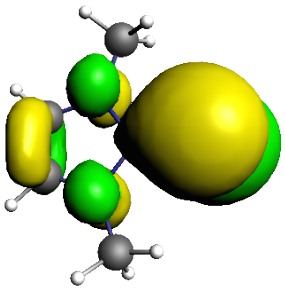 HOMO-1 (ε = 28.82)	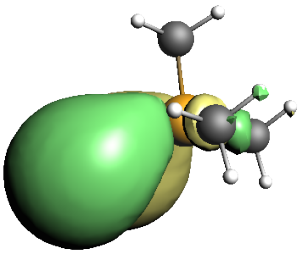 LUMO (ε = -174.10)
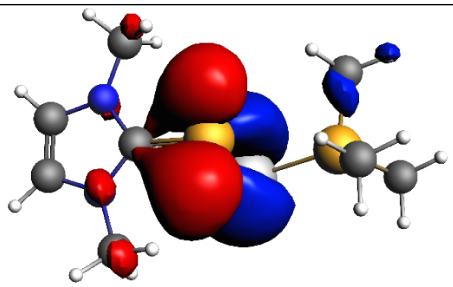 $\Delta\rho_{(2)}$ $\Delta E_{orb(2)}$ = -24.5; $\lvert\nu_{2\alpha}/\nu_{2\beta}\rvert$ = 0.27/0.27	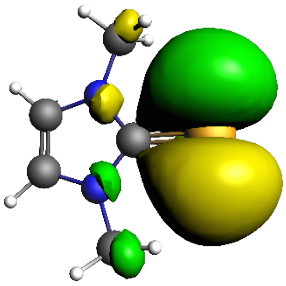 HOMO (ε = 38.74)	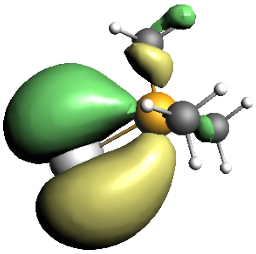 LUMO+1 (ε = -172.72)

Figure S18. The shape of the deformation densities $\Delta\rho_{(1)-(2)}$ that correspond to $\Delta E_{orb(1)-(2)}$, and the associated MOs of (NHC)P-Ga(PMe_3) (**5**) and the fragments orbitals of $[(NHC)P]^-$ and $[Ga(PMe_3)]^+$ in the singlet state at the BP86-D3(BJ)/TZ2P level. Isosurface values are 0.003 au for $\Delta\rho_{(1)}$ and isosurface value 0.001 for $\Delta\rho_{(2)}$. The eigenvalues $|\nu_n|$ give the size of the charge migration in e. The direction of the charge flow of the deformation densities is red→blue. Energy values are in kcal/mol.

(NHC)P-Ga(NHC) (**6**)	$[(NHC)P]^-$ (S)	$[Ga(NHC)]^+$ (S)
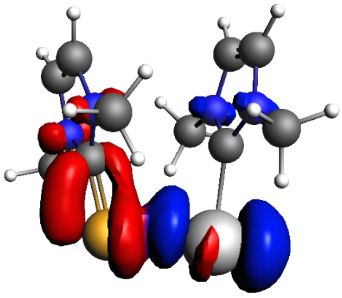 $\Delta\rho_{(1)}$ $\Delta E_{orb(1)}$ = -61.0; $\lvert\nu_{1\alpha}/\nu_{1\beta}\rvert$ = 0.45/0.45	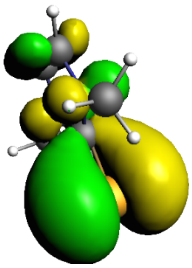 HOMO-1 (ε = 28.59)	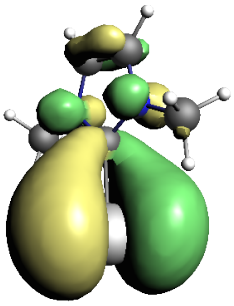 LUMO (ε = -160.27)
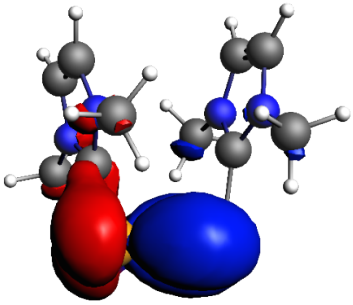 $\Delta\rho_{(2)}$ $\Delta E_{orb(2)}$ = -21.1; $\lvert\nu_{2\alpha}/\nu_{2\beta}\rvert$ = 0.27/0.27	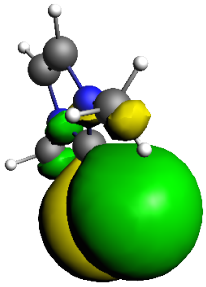 HOMO (ε = -29.74)	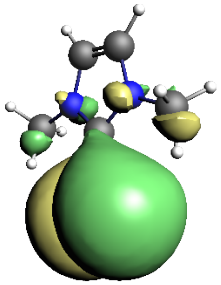 LUMO+1 (ε = -157.50)

Figure S19. The shape of the deformation densities $\Delta\rho_{(1)-(2)}$ that correspond to $\Delta E_{orb(1)-(2)}$, and the associated MOs of (NHC)P-Ga(NHC) (**6**) and the fragments orbitals of $[(NHC)P]^-$ and $[Ga(NHC)]^+$ in the singlet state at the BP86-D3(BJ)/TZ2P level. Isosurface values are 0.003 au for $\Delta\rho_{(1)}$ and isosurface value 0.001 for $\Delta\rho_{(2)}$. The eigenvalues $|\nu_n|$ give the size of the charge migration in e. The direction of the charge flow of the deformation densities is red→blue. Energy values are in kcal/mol.

$(PMe_3)P\text{-}Ga(PMe_3)$ (**7**)	$[(PMe_3)P]^-$ (S)	$[Ga(PMe_3)]^+$ (S)
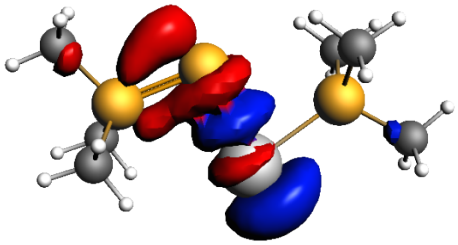 $\Delta\rho_{(1)}$ $\Delta E_{orb(1)}$ = -74.8; $\lvert\nu_{1\alpha}/\nu_{1\beta}\rvert$ = 0.46/0.46	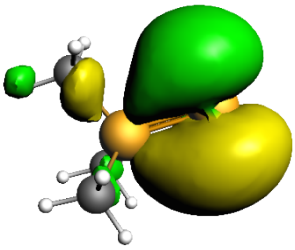 HOMO (ε = 29.74)	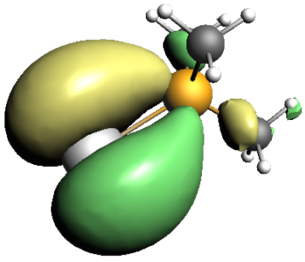 LUMO (ε = -173.41)
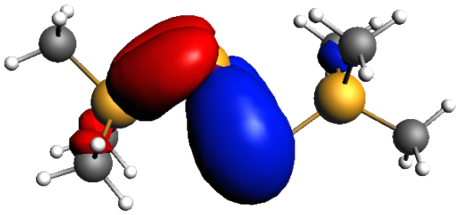 $\Delta\rho_{(2)}$ $\Delta E_{orb(2)}$ = -21.0; $\lvert\nu_{2\alpha}/\nu_{2\beta}\rvert$ = 0.27/0.27	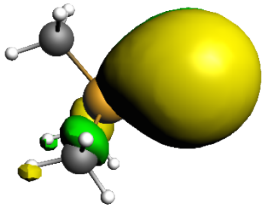 HOMO-1 (ε = 29.29)	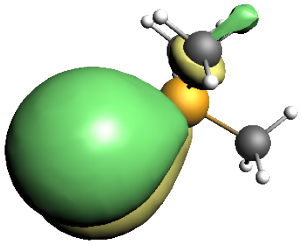 LUMO+1 (ε = -172.95)

Figure S20. The shape of the deformation densities $\Delta\rho_{(1)\text{-}(2)}$ that correspond to $\Delta E_{orb(1)\text{-}(2)}$, and the associated MOs of $(PMe_3)P\text{-}Ga(PMe_3)$ (**7**) and the fragments orbitals of $[(PMe_3)P]^-$ and $[Ga(PMe_3)]^+$ in the singlet state at the BP86-D3(BJ)/TZ2P level. Isosurface values are 0.003 au for $\Delta\rho_{(1)}$ and isosurface value 0.001 for $\Delta\rho_{(2)}$. The eigenvalues $|\nu_n|$ give the size of the charge migration in e. The direction of the charge flow of the deformation densities is red→blue. Energy values are in kcal/mol.

We have performed EDA-NOCV[5] to study the electronic state and nature of interaction between $[(NHC^{DMP})_2]$ and [P-Ga] fragments of **6′**. We considered two different bonding possibilities, neutral fragments of $[(NHC^{DMP})_2]$ and [P-Ga] in singlet state forming dative bond and singly charged fragments of $[(NHC^{DMP})_2]^+$ and $[P\text{-}Ga]^-$ in doublet state interacting to form σ electron sharing and π dative bond. Out of the three bonding possibilities tried, it was found that the least ΔE_{orb} was found for the dative bonding possibility. The contribution of ΔE_{elstat} (49.5%) predominates in the total attractive interactions. ΔE_{orb} and ΔE_{disp} contributes 44.1% and 5.6% to the total attractive interactions. ΔE_{orb} can be further divided into pairwise contribution. $\Delta E_{orb(1)}$ contributing 54.5% of the total orbital interactions, represents a strong σ-donation from HOMO-1 of $[(NHC^{DMP})_2]$ to the LUMO of PGa unit. $\Delta E_{orb(2)}$ (16.5%) is weaker σ-donation from HOMO of $[(NHC^{DMP})_2]$ to the LUMO+1 of PGa unit. $\Delta E_{orb(3)}$ (12.5%) shows the π-backdonation from HOMO-1 of PGa moiety to LUMO+8 of $[(NHC^{DMP})_2]$. $\Delta E_{orb(4)}$ (6.5%) is very weaker backdonation from HOMO pf PGa moiety to LUMO+10 of $[(NHC^{DMP})_2]$.

Table S15. EDA-NOCV results of NHC^{DMP}-P-Ga-NHC^{DMP} (**6′**) using two different sets of fragments with different charges and electronic states (S = singlet, D = doublet) and associated bond types at the BP86-D3(BJ)/TZ2P level. Energies are in kcal/mol. The most favourable fragmentation scheme and bond type is given by the smallest ΔE_{orb} value written in bold.

Molecule	**Bond type[a]**	**Fragments**	ΔE_{int}	ΔE_{Pauli}	ΔE_{elstat}	ΔE_{disp}	ΔE_{orb}
NHC^{DMP}-P-Ga-NHC^{DMP} (**6′**)	D	$[(NHC^{DMP})_2]$ (S) + PGa (S)	-149.6	424.8	-284.5	-32.0	**-257.8**
	D+E	$[(NHC^{DMP})_2]^+$ (D) + $[PGa]^-$ (D)	-227.6	499.3	-375.4	-32.0	-319.5

Table S16. The EDA-NOCV results at the BP86-D3(BJ)/TZ2P level of L–PGa–L′ bonds of NHC^{DMP}-P-Ga-NHC^{DMP} (**6′**) using [ligands] and [P-Ga] in the electronic singlet (S) states as interacting fragments. Energies are in kcal/mol.

Energy	**Interaction**	**$[(NHC^{DMP})_2]$ (S) + [P-Ga] (S)**
ΔE_{int}		-149.6
ΔE_{Pauli}		424.8
ΔE_{disp}[a]		-32.0 (5.6%)
ΔE_{elstat}[a]		-284.5 (49.5%)
ΔE_{orb}[a]		-257.8 (44.1%)
$\Delta E_{orb(1)}$[b]	L→P-Ga←L′ σ donation	-140.4 (54.5%)
$\Delta E_{orb(2)}$[b]	L→P-Ga←L′ σ donation	-42.6 (16.5%)
$\Delta E_{orb(3)}$[b]	L←P-Ga→L′ π backdonation	-32.3 (12.5%)
$\Delta E_{orb(4)}$[b]	L←P-Ga→L′ π backdonation	-16.9 (6.5%)
$\Delta E_{orb(rest)}$		-25.6 (10.0%)

NHC^{DMP}-PGa-NHC^{DMP}	$[(NHC^{DMP})_2]$ (S)	[P-Ga] (S)
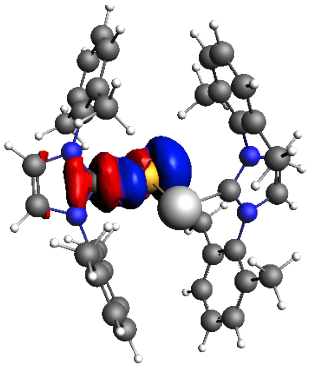	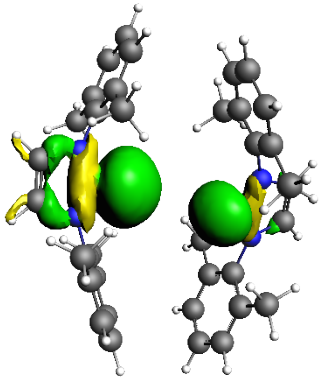	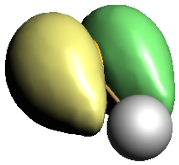
$\Delta\rho_{(1)}$	HOMO-1 (ε = -107.23)	LUMO (ε = -137.90)
$\Delta E_{orb(1)}$ = -140.4; $\lvert\nu_{1\alpha}/\nu_{1\beta}\rvert$ = 0.48/0.48		
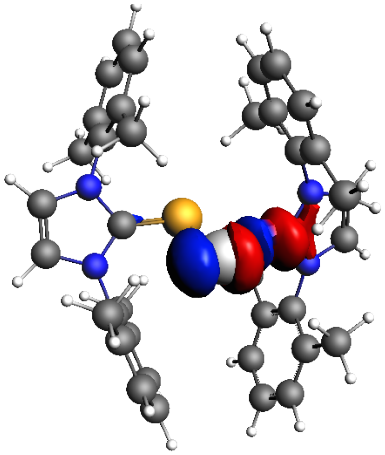	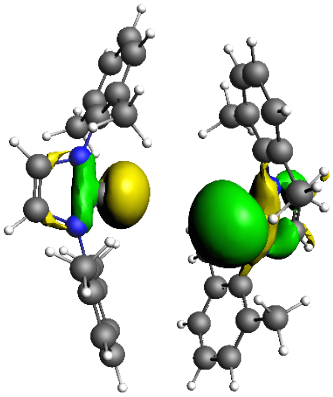	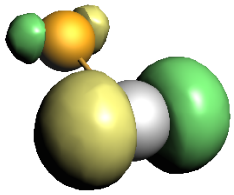
$\Delta\rho_{(2)}$	HOMO (ε = -101.92)	LUMO+1 (ε = -53.50)
$\Delta E_{orb(2)}$ = -42.6; $\lvert\nu_{2\alpha}/\nu_{2\beta}\rvert$ = 0.37/0.37		
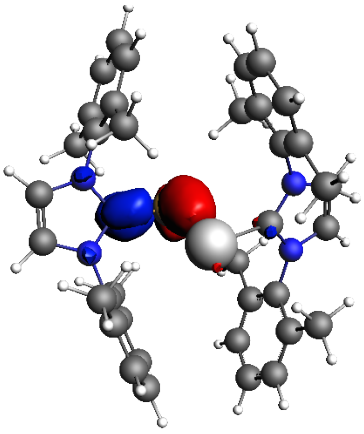	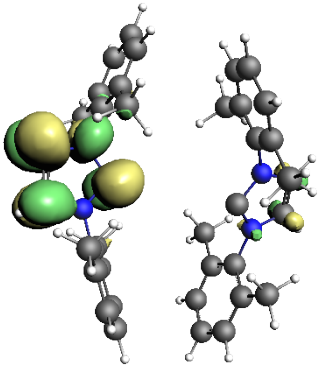	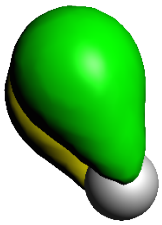
$\Delta\rho_{(3)}$	LUMO+8 (ε = -148.97)	HOMO-1 (ε = - 122.91)
$\Delta E_{orb(3)}$ = -32.3; $\lvert\nu_{3\alpha}/\nu_{3\beta}\rvert$ = 0.31/0.31		

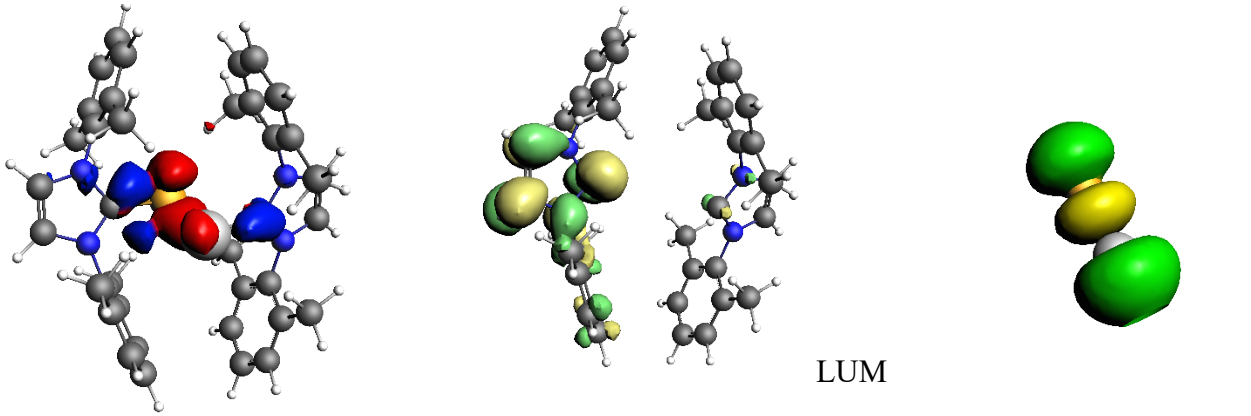

Figure 21. The shape of the deformation densities $\Delta\rho_{(1)-(4)}$ that correspond to $\Delta E_{orb(1)-(4)}$, and the associated MOs of NHC^{DMP}-P-Ga-NHC^{DMP} (**6′**) and the fragments orbitals of [$(NHC^{DMP})_2$] and [P-Ga] in the Singlet state (S) at the BP86-D3(BJ)/TZ2P level. Isosurface values are 0.003 au for $\Delta\rho_{(1-3)}$, and 0.001 au for $\Delta\rho_{(4)}$. The eigenvalues $|\nu_n|$ give the size of the charge migration in e. The direction of the charge flow of the deformation densities is red→blue. Energy values are in kcal/mol.

Table S17. EDA-NOCV results of $(cAAC)_2GaP{-}Fe(CO)_4$ bond of $(cAAC)_2GaP$-$Fe(CO)_4$ (**8**) complex using three different sets of fragments with different charges and electronic states (S = singlet, D = doublet, T = triplet) and associated bond types at the BP86-D3(BJ)/TZ2P level. Energies are in kcal/mol. The most favourable fragmentation scheme and bond type is given by the smallest ΔE_{orb} value written in bold.

Molecule	**Bond type**[a]	**Fragments**	ΔE_{int}	ΔE_{Pauli}	ΔE_{elstat}	ΔE_{disp}	ΔE_{orb}
$(cAAC)_2GaP$-$Fe(CO)_4$ (**8**)	D	$(cAAC)_2PGa$ (S) + $Fe(CO)_4$ (S)	-72.4	136.7	-102.7	-21.9	**-84.4**
	E (σ)	$[(cAAC)_2PGa]^+$ (D) + $[Fe(CO)_4]^-$ (D)	-128.6	171.9	-163.2	-21.9	-115.4
	E (σ, π)	$(cAAC)_2PGa$ (T) + $Fe(CO)_4$ (T)	129.8	173.6	-114.4	-21.9	-167.1

Table S18. The EDA-NOCV results at the BP86-D3(BJ)/TZ2P level of $(cAAC)_2GaP{-}Fe(CO)_4$ bond of $(cAAC)_2GaP\text{-}Fe(CO)_4$ (**8**) complex using $[(cAAC)_2GaP]$ and $[Fe(CO)_4]$ in the electronic singlet (S) states as interacting fragments. Energies are in kcal/mol.

Energy	**Interaction**	**$(cAAC)_2PGa$ (S) + $Fe(CO)_4$ (S)**
ΔE_{int}		-72.4
ΔE_{Pauli}		136.7
ΔE_{disp}[a]		-21.9 (10.5%)
ΔE_{elstat}[a]		-102.7 (49.1%)
ΔE_{orb}[a]		-84.4 (40.4%)
$\Delta E_{orb(1)}$[b]	$(cAAC)_2GaP \rightarrow Fe(CO)_4$ σ-donation	-56.2 (66.6%)
$\Delta E_{orb(2)}$[b]	$(cAAC)_2GaP \leftarrow Fe(CO)_4$ π-backdonation	-8.2 (9.7%)
$\Delta E_{orb(rest)}$		-20.0 (23.7%)

[a]The values in the parentheses show the contribution to the total attractive interaction $\Delta E_{elstat} + \Delta E_{orb} + \Delta E_{disp}$.

[b]The values in parentheses show the contribution to the total orbital interaction ΔE_{orb}.

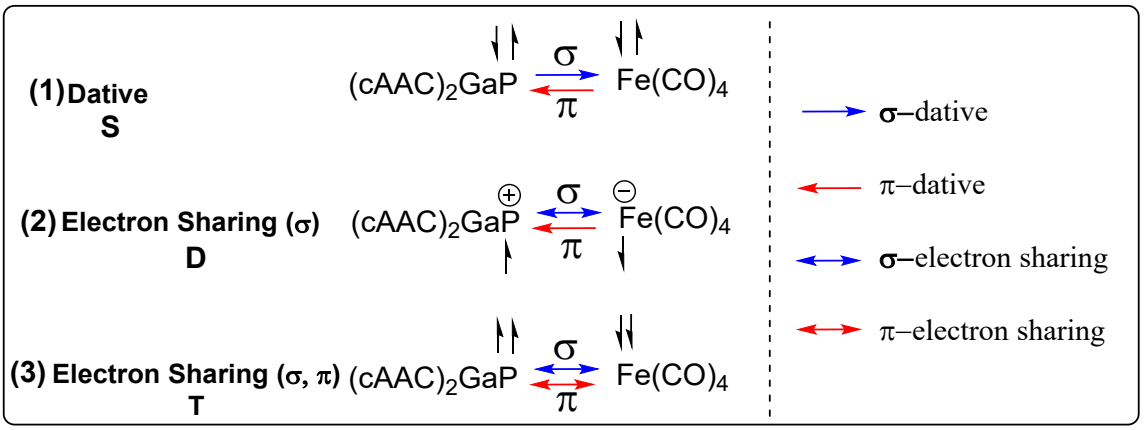

Scheme S1. Bonding possibilities representing P – Fe bond in $(cAAC)_2GaP{-}Fe(CO)_4$ (**8**)

We have performed EDA-NOCV[5] to study the electronic state and nature of interaction between $(cAAC)_2GaP$ and $Fe(CO)_4$ fragments of **8**. We considered three different bonding possibilities (Scheme S1), neutral fragments of $(cAAC)_2GaP$ and $Fe(CO)_4$ in singlet state forming dative bond, singly charged fragments of $[(cAAC)_2PGa]^+$ and $[Fe(CO)_4]^-$ in doublet state interacting to form σ electron sharing and π dative bond and neutral fragments of $(cAAC)_2GaP$ and $Fe(CO)_4$ in triplet state froming electron sharing bond. Out of the three bonding possibilities tried, it was found that the least ΔE_{orb} was found for the dative bonding possibility. The contribution of ΔE_{elstat} (49.1%) predominates in the total attractive interactions indicating the electrostatic nature of P – Fe bond. ΔE_{orb} and ΔE_{disp} contributes 40.4% and 10.5% to the total attractive interactions. ΔE_{orb} can be further divided into pairwise contribution. $\Delta E_{orb(1)}$ contributing 66.6% of the total orbital interactions, represents a strong σ-donation from HOMO of $(cAAC)_2GaP$ to the LUMO of $Fe(CO)_4$. $\Delta E_{orb(2)}$ (9.9%) shows the π-backdonation from HOMO of Fe to LUMO+2 of P.

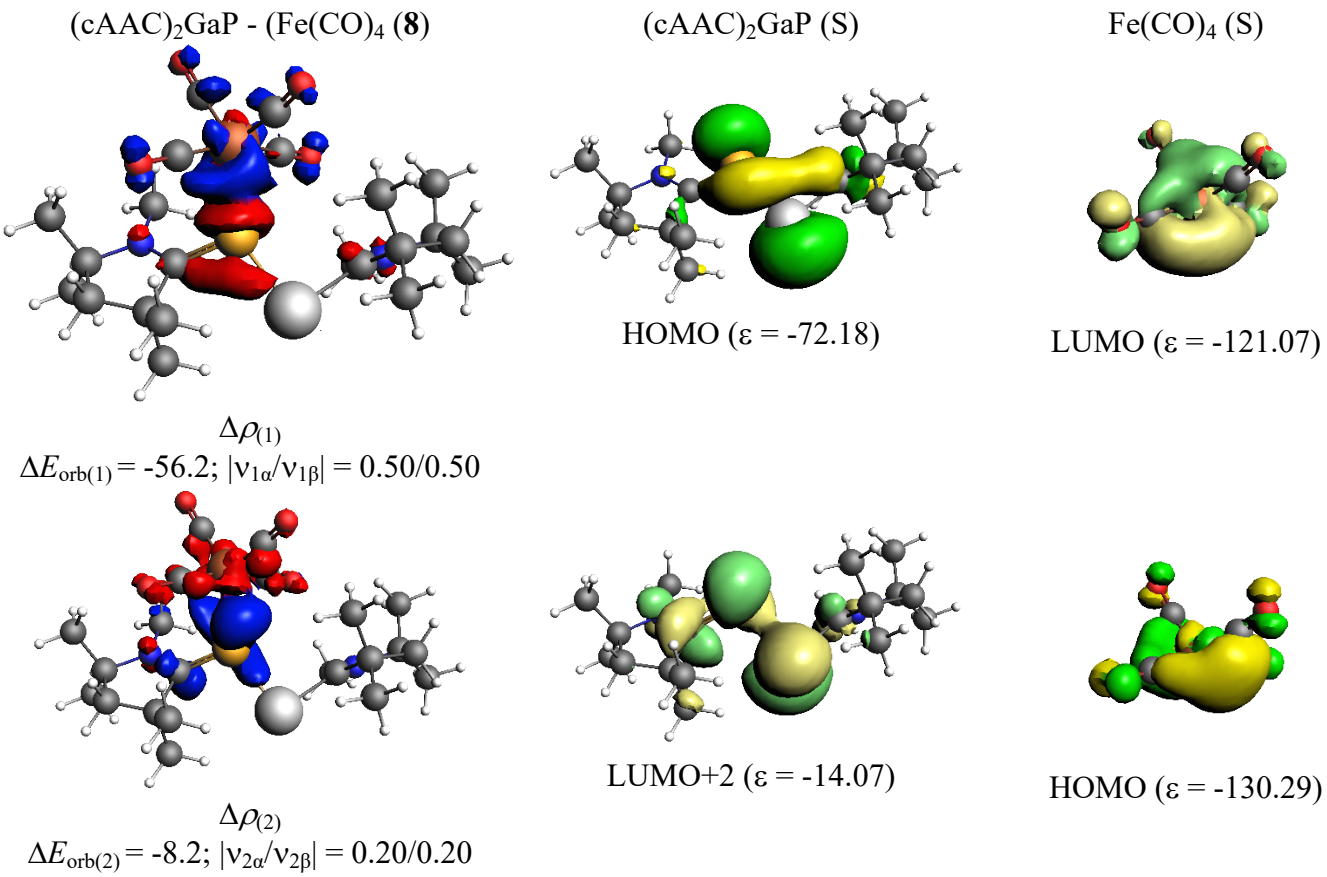

Figure 22. The shape of the deformation densities $\Delta\rho_{(1)-(4)}$ that correspond to $\Delta E_{orb(1)-(2)}$, and the associated MOs of $(cAAC)_2GaP{-}(Fe(CO)_4$ (**8**) and the fragments orbitals of $(cAAC)_2GaP$ and $[(Fe(CO)_4]$ in the Singlet state (S) at the BP86-D3(BJ)/TZ2P level. Isosurface values are 0.003 au for

$\Delta\rho_{(1)}$ and 0.0007 au for $\Delta\rho_{(2)}$. The eigenvalues $|\nu_n|$ give the size of the charge migration in e. The direction of the charge flow of the deformation densities is red→blue. Energy values are in kcal/mol.

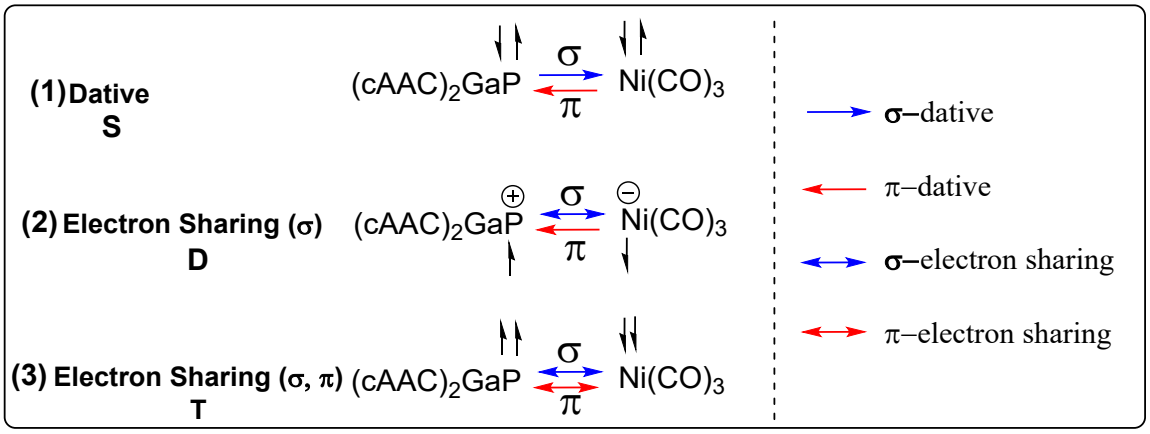

Scheme S2. Bonding possibilities representing P–Ni bond in $(cAAC)_2GaP{-}Ni(CO)_3$ (**9**)

Table S19. EDA-NOCV results of $(cAAC)_2GaP{-}Ni(CO)_3$ bond of $(cAAC)_2GaP$-$Ni(CO)_3$ (**9**) complex using three different sets of fragments with different charges and electronic states (S = singlet, D = doublet, T = triplet) and associated bond types at the BP86-D3(BJ)/TZ2P level. Energies are in kcal/mol. The most favourable fragmentation scheme and bond type is given by the smallest ΔE_{orb} value written in bold.

Molecule	**Bond type**[a]	**Fragments**	ΔE_{int}	ΔE_{Pauli}	ΔE_{elstat}	ΔE_{disp}	ΔE_{orb}
$(cAAC)_2GaP$-$Ni(CO)_3$ (**9**)	D	$(cAAC)_2PGa$ (S) + $Ni(CO)_3$ (S)	-50.5	103.6	-84.2	-18.3	**-51.6**
	E (σ)	$[(cAAC)_2PGa]^+$ (D) + $[Ni(CO)_3]^-$ (D)	-140.2	136.5	-149.5	-18.3	-108.9
	E (σ, π)	$(cAAC)_2PGa$ (T) + $Ni(CO)_3$ (T)	-162.3	132.3	-92.4	-18.3	-183.9

We have performed EDA-NOCV[5] studies to find the best bonding description of the P – Ni bond. We considered three different bonding possibilities (Scheme S2), neutral fragments of $(cAAC)_2GaP$ and $Ni(CO)_3$ in singlet state forming dative bond, singly charged fragments of $[(cAAC)_2PGa]^+$ and $[Ni(CO)_3]^-$ in doublet state interacting to form σ electron sharing and π dative bond and neutral fragments of $(cAAC)_2GaP$ and $Ni(CO)_3$ in triplet state froming electron

sharing bond. It was observed that when the neutral fragments of $(cAAC)_2GaP$ and $Ni(CO)_3$ interacted to form dative (Scheme S2) was found to have the least ΔE_{orb} and thus it was considered to the best bonding scenario. The contribution of ΔE_{elstat} (54.6%) predominates in the total attractive interactions indicating the electrostatic nature of P–Fe bond. ΔE_{orb} and ΔE_{disp} contributes 33.5% and 11.9% to the total attractive interactions. ΔE_{orb} can be further divided into pairwise contribution. $\Delta E_{orb(1)}$ represents a strong σ-donation from HOMO of $(cAAC)_2GaP$ to the LUMO of $Ni(CO)_3$, contributing 66.6% of the total orbital interactions. $\Delta E_{orb(2)}$ and $\Delta E_{orb(3)}$ (10.1 and 9.9%, respectively) show the π-backdonation from HOMO-1 of $Ni(CO)_3$ to LUMO+2 of P and HOMO of $Ni(CO)_3$ to LUMO+2 of P, respectively.

Table S20. The EDA-NOCV results at the BP86-D3(BJ)/TZ2P level of $(cAAC)_2GaP{-}Ni(CO)_3$ bond of $(cAAC)_2GaP{-}Ni(CO)_3$ (**10**) complex using $[(cAAC)_2GaP]$ and $[Ni(CO)_3]$ in the electronic singlet (S) states as interacting fragments. Energies are in kcal/mol.

Energy	**Interaction**	**$(cAAC)_2PGa$ (S) + $Ni(CO)_3$ (S)**
ΔE_{int}		-50.6
ΔE_{Pauli}		103.6
ΔE_{disp}[a]		-18.3 (11.9%)
ΔE_{elstat}[a]		-84.2 (54.6%)
ΔE_{orb}[a]		-51.6 (33.5%)
$\Delta E_{orb(1)}$[b]	$(cAAC)_2GaP \rightarrow Ni(CO)_3$ σ-donation	-32.6 (63.1%)
$\Delta E_{orb(2)}$[b]	$(cAAC)_2GaP \leftarrow Ni(CO)_3$ π-backdonation	-5.2 (10.1%)
$\Delta E_{orb(2)}$[b]	$(cAAC)_2GaP \leftarrow Ni(CO)_3$ π-backdonation	-5.1 (9.9%)
$\Delta E_{orb(rest)}$		-8.7 (16.9%)

[a]The values in the parentheses show the contribution to the total attractive interaction $\Delta E_{elstat} + \Delta E_{orb} + \Delta E_{disp}$.

[b]The values in parentheses show the contribution to the total orbital interaction ΔE_{orb}.

$(cAAC)_2GaP$ - $(Ni(CO)_3)$ (**10**)	$(cAAC)_2GaP$ (S)	$Ni(CO)_3$ (S)
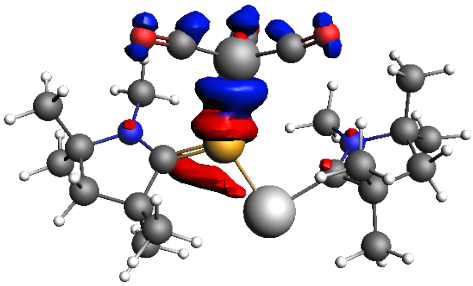 $\Delta\rho_{(1)}$ $\Delta E_{orb(1)}$ = -32.6; $\lvert\nu_{1\alpha}/\nu_{1\beta}\rvert$ = 0.39/0.39	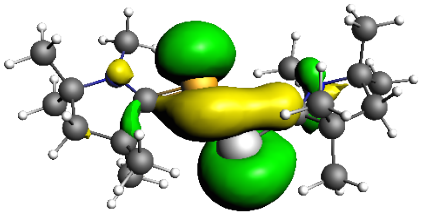 HOMO (ε = -74.95)	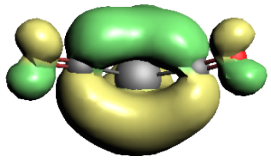 LUMO (ε = -90.17)
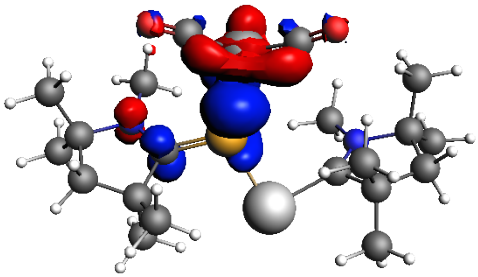 $\Delta\rho_{(2)}$ $\Delta E_{orb(2)}$ = -5.2; $\lvert\nu_{2\alpha}/\nu_{2\beta}\rvert$ = 0.12/0.12	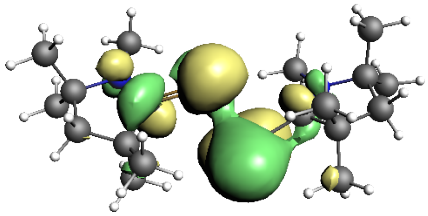 LUMO+2 (ε = -13.14)	 HOMO-1 (ε = -145.97)
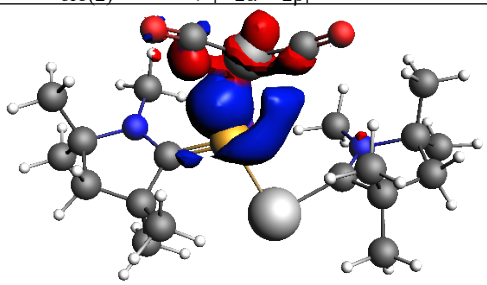 $\Delta\rho_{(2)}$ $\Delta E_{orb(2)}$ = -5.1; $\lvert\nu_{3\alpha}/\nu_{3\beta}\rvert$ = 0.10/0.10	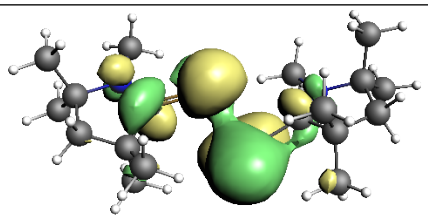 LUMO+2 (ε = -13.14)	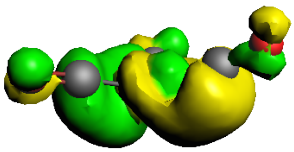 HOMO (ε = -142.74)

Figure 23. The shape of the deformation densities $\Delta\rho_{(1)-(4)}$ that correspond to $\Delta E_{orb(1)-(2)}$, and the associated MOs of $(cAAC)_2GaP$ - $Ni(CO)_3$ (**10**) and the fragments orbitals of $(cAAC)_2GaP$ and $[Ni(CO)_3]$ in the Singlet state (S) at the BP86-D3(BJ)/TZ2P level. Isosurface values are 0.003 au for $\Delta\rho_{(1)}$ and 0.0003 au for $\Delta\rho_{(2-3)}$. The eigenvalues $\lvert\nu_n\rvert$ give the size of the charge migration in e. The direction of the charge flow of the deformation densities is red→blue. Energy values are in kcal/mol.

Table S21. The EDA-NOCV results at the M06-2X/TZ2P level for $(cAAC)_2GaP{-}M(CO)_n$ bond of $(cAAC)_2GaP{-}M(CO)_n$ complex [M = Fe, n = 4 (**8**); M = Ni, n = 3 (**9**)] using $[(cAAC)_2GaP]$ and $[M(CO)_n]$ in the electronic singlet (S) states as interacting fragments. Energies are in kcal/mol.

Energy	**Interaction**	**$(cAAC)_2PGa$ (S) + $Fe(CO)_4$ (S)**	**$(cAAC)_2PGa$ (S) + $NI(CO)_3$ (S)**
ΔE_{int}		-43.9	-30.0
ΔE_{Pauli}		88.2	64.6
ΔE_{disp}[a]		-1.7 (1.1%)	-1.5 (1.4%)
ΔE_{elstat}[a]		-84.3 (56.7%)	-64.6 (59.6%)
ΔE_{orb}[a]		-62.6 (42.1%)	-42.3 (39.0%)
$\Delta E_{orb(1)}$[b]	$(cAAC)_2GaP \rightarrow M(CO)_n$ σ-donation	-42.3 (66.6%)	-29.4 (69.5)
$\Delta E_{orb(2)}$[b]	$(cAAC)_2GaP \leftarrow M(CO)_n$ π-backdonation	-5.8 (9.7%)	

[a]The values in the parentheses show the contribution to the total attractive interaction $\Delta E_{elstat} + \Delta E_{orb} + \Delta E_{disp}$.

[b]The values in parentheses show the contribution to the total orbital interaction ΔE_{orb}.

Table S22. NBO results of the compound NHC^{DMP}–P–Ga–NHC^{DMP} (**8**) at the BP86-D3(BJ)/def2-TZVPP level of theory. Occupation number (ON), polarization and hybridization of the L–P, P–Ga and Ga–L′ bonds

	Bond	**ON**	**Polarization and hybridization (%)**		**WBI**	**q**	
						P	Ga
Compound **6′**	C43-P1	1.96	P: 32.3 s(15.7), p(83.5)	C: 67.7 s(45.0), p(54.7)	1.13		
	P1 – Ga80	1.82	P: 83.0 s(11.8), p(87.7)	Ga: 17 s(6.0), p(93.8)	0.78	-0.45	0.25
	Ga80 – C6	1.91	C: 87.5 s(44.8), p(55.2)	Ga: 13.5 s(5.8), p(93.8)	0.44		

Table S23. NBO results of the compounds cAAC–P–Ga–cAAC^{Me} (**1**), cAAC–P–Ga–NHC^{Me} (**2**), cAAC–P–Ga–PMe_3 (**3**), NHC^{Me}–P–Ga–cAAC^{Me} (**4**), NHC^{Me}–P–Ga–PMe_3 (**5**), NHC^{Me}–P–Ga–NHC^{Me} (**6**) and PMe_3–P–Ga–PMe_3 (**7**) at the B3LYP/def2-TZVPP level of theory. Occupation number (ON), polarization and hybridization of the L–P, P–Ga and Ga–L′ bonds.

Compound	Bond	ON	Polarization and hybridization (%)		WBI	q	
						P	Ga
1	C25-P24	1.97	P: 33.4 s(20.2), p(79.0)	C: 66.6 s(40.3), p(59.3)	1.49	-0.34	0.34
		1.89	P: 61.8 s(0.1), p(99.5)	C: 38.2 s(0.0), p(99.8)			
	P24 – Ga56	1.83	P: 77.5 s(16.7), p(82.6)	Ga: 22.5 s(9.3), p(90.3)	0.76		
	Ga56 – C3	1.91	C: 87.9 s(39.0), p(60.9)	Ga: 12.1 s(7.2), p(92.2)	0.55		
2	P10 – C11	1.88	P: 61.5 s(0.1), p(99.5)	C: 38.2 s(0.0), p(99.8)	1.49	-0.3	0.24
		1.97	P: 33.5 s(20.5), p(78.7)	C: 66.5 s(40.4), p(59.2)			
	P10 – Ga44	1.89	P: 77.6% s(17.0), p(82.3)	Ga: 22.4% s(8.6), p(91.0)	0.80		
	Ga44 – C2	1.93	C: 87.6% s(41.1), p(58.9)	Ga: 12.4% s(4.9), p(94.4)	0.46		
3	P28 – C3	1.97	P: 33.9 s(21.2), p(78.1)	C:66.1 s(40.2), p(59.4)	1.49	-0.44	0.25
		1.88	P: 61.9 s(0.0), p(99.5)	C: 38.1 s(0.0), p(99.7)			
	P28 – Ga42	1.92	P: 78.7 s(16.3), p(83.0)	Ga: 21.2 S(7.9), p(91.8)	0.81		
	Ga42 – P29	1.91	P: 89.0 s(29.2), p(70.8)	Ga: 11 S(2.2), p(97.2)	0.37		
4	P12 – C13	1.97	P: 31.9 s(15.8), p(83.3)	C:68.1 s(43.6), p(56.1)	1.24	-0.50	0.28
	P12 –	1.84	P: 81.2 s(16.6), p(82.8)	Ga: 18.8 s(6.9), p(92.6)	0.86		

	Ga11						
	Ga11 – C4	1.91	C: 87.5 s(39.2), p(60.7)	Ga: 12.5 s(7.4), p(91.9)	0.56		
5	P2 – C3	1.97	P: 32.1 s(15.5), p(83.6)	C:67.9 s(43.6), p(56.1)	1.21	-0.59	0.20
	P2 – Ga1	1.88	P: 84.5 s(6.9), p(92.5)	Ga: 15.5 s(3.4), p(96.2)	0.93		
	Ga1 – P10	1.90	P: 88.9 s(29.7), p(70.2)	Ga: 11.1 s(2.5), p(96.9)	0.38		
6	C11 – P10	1.97	P: 31.8 s(16.0), p(83.1)	C:68.2 s(44.5), p(55.2)	1.27	-0.47	0.24
	P10 – Ga32	1.84	P: 85.2 s(5.8), p(93.7)	Ga: 14.8 s(3.1), p(96.4)	0.92		
	Ga32 – C2	1.93	C: 88.4 s(40.9), p(59.1)	Ga: 11.6 s(4.6), p(94.9)	0.44		
7	P15 – P1	1.97	P15: 59.3 s(32.5), p(66.9)	P1: 40.7 s(13.9), p(84.7)	1.26	-0.87	0.20
	P1 – Ga28	1.87	P: 79.6 s(13.9), p(84.9)	Ga: 20.4 s(8.6), p(91.2)	0.89		
		1.80	P: 90.0 s(0.0), p(99.5)	Ga: 10.0 s(0.0), p(99.4)			
	Ga28 – P2				0.41		

Table 24. NBO results of the compounds cAAC–P–Ga–cAAC^{Me} (**1**), cAAC–P–Ga–NHC^{Me} (**2**), cAAC–P–Ga–PMe_3 (**3**), NHC^{Me}–P–Ga–cAAC^{Me} (**4**), NHC^{Me}–P–Ga–PMe_3 (**5**), NHC^{Me}–P–Ga–NHC^{Me} (**6**) and PMe_3–P–Ga–PMe_3 (**7**) at the M06-2X/def2-TZVPP level of theory. Occupation number (ON), polarization and hybridization of the L–P, P–Ga and Ga–L′ bonds.

Compound	**Bond**	**ON**	**Polarization and hybridization (%)**		**WBI**	**q**	
						P	Ga
1	C25-P24	1.97	P: 33.5 s(22.4), p(76.9)	C: 66.5 s(40.7), p(58.9)	1.52	-0.41	0.39
		1.91	P: 61.6 s(0.0), p(99.5)	C: 38.4 s(0.0), p(99.7)			
	P24 – Ga56	1.83	P: 80.3 s(19.0), p(80.2)	Ga: 19.7 s(8.2), p(91.1)	0.66		
	Ga56 – C3	1.91	C: 90.0	Ga: 10.0	0.40		

			s(39.2), p(60.7)	s(6.9), p(92.3)			
2	P10 – C11	1.90	P: 62.9 s(0.0), p(99.5)	C: 37.1 s(0.0), p(99.8)	1.49	-0.45	0.30
		1.97	P: 33.3 s(21.7), p(77.6)	C: 66.7 s(40.6), p(59.1)			
	P10 – Ga44	1.90	P: 79.2% s(19.9), p(79.3)	Ga: 20.8% S(9.0), p(90.7)	0.74		
	Ga44 – C2	1.93	C: 88.8% s(41.3), p(58.6)	Ga: 11.2% s(5.4), p(94.0)	0.41		
3	P28 – C3	1.97	P: 33.7 s(21.9), p(77.2)	C:66.3 s(40.3), p(59.3)	1.49	-0.50	0.32
		1.89	P: 63.4 s(0.0), p(99.4)	C: 36.6 s(0.0), p(99.7)			
	P28 – Ga42	1.92	P: 79.9 s(18.9), p(80.1)	Ga: 20.1 S(9.1), p(90.5)	0.75		
	Ga42 – P29	1.91	P: 90.1 s(29.5), p(70.4)	Ga: 9.9 S(2.3), p(96.9)	0.34		
4	P12 – C13	1.97	P: 31.5 s(16.3), p(82.8)	C:68.5 s(43.6), p(56.1)	1.20	-0.61	0.32
	P12 – Ga11	1.86	P: 84.2 s(19.0), p(80.3)	Ga: 15.7 s(5.8), p(93.3)	0.78		
	Ga11 – C4	1.91	C: 89.3 s(39.6), p(60.4)	Ga: 10.7 s(7.4), p(91.8)	0.43		
5	P2 – C3	1.97	P: 31.7 s(15.4), p(83.6)	C:68.3 s(43.6), p(56.2)	1.19	-0.67	0.26
	P2 – Ga1	1.90	P: 84.3 s(12,0), p(87.1)	Ga: 15.7 s(6.9), p(92.6)	0.87		
	Ga1 – P10	1.91	P: 89.8 s(30.1), p(69.8)	Ga: 10.2 s(2.9), p(96.3)	0.36		
6	C11 – P10	1.97	P: 31.3 s(16.7), p(82.4)	C:68.7 s(44.5), p(55.2)	1.27	-0.55	0.30
	P10 – Ga32	1.86	P: 84.3 s(13.2), p(86.2)	Ga: 15.7 s(6.7), p(92.6)	0.86		
	Ga32 – C2	1.94	C: 89.5 s(41.2), p(58.8)	Ga: 10.5 s(4.9), p(94.5)	0.41		
7	P15 – P1	1.97	P15: 59.9 s(32.7), p(66.7)	P1: 40.1 s(13.9), p(84.6)	1.26	-0.92	0.27

	P1 – Ga28	1.89	P: 80.4 s(15.6), p(83.0)	Ga: 19.6 s(10.0), p(89.8)	0.84		
		1.81	P: 91.6 s(0.0), p(99.3)	Ga: 8.3 s(0.0), p(99.9)			
	Ga28 – P2				0.38		

We have conducted NBO analysis in three different levels, BP86/def2-TZVPP, B3LYP/def2-TZVPP and M06-2X/def2-TZVPP. The results obtained in the three levels are very similar expect for the fact that we observed two different bonding occupancies for P−Ga bond of PGa moiety for the compound **7** in B3LYP/def2-TZVPP and M06-2X/def2-TZVPP. Both occupancies are polarized towards P (80-90%).

References:

1. (a) A. D. Becke, Phys. Rev. A: At., Mol., Opt. Phys., 1988, 38, 3098-3100. (b) J. P. Perdew, Phys. Rev. B: Condens. Matter Mater. Phys., 1986, 33, 8822-8824. (b) C. Lee, W. Yang and R. G. Parr, *Phys. Rev. B*, 1988, **37**, 785-789. (c) Y. Zhao and D. G. Truhlar, *Theor. Chem. Account.*, 2008, **120**, 215-241.
2. M. J. Frisch, et al., Gaussian 16, Revision A.03, Gaussian, Inc., Wallingford CT, 2016.
3. (a) K. B. Wiberg, *Tetrahedron*, 1968, **24**, 1083-1096. (b) F. Weinhold and C. Landis, *Valency and Bonding, A Natural Bond Orbital Donor-Acceptor Perspective*, Cambridge University Press, Cambridge, 2005. (*c*) C. R. Landis and F. Weinhold, The NBO View of Chemical Bonding, *The Chemical Bond: Fundamental Aspects of Chemical Bonding*, G. Frenking and S. Shaik, Wiley, 2014, pp. 91-120. (d) A. E. Reed, L. A. Curtiss and F. Weinhold, *Chemical Reviews*, 1988, **88**, 899-926.
4. AIMAll (Version 10.05.04), T. A. Keith, 2010 (aim.tkgristmill.com)
5. M. A. Celik, R. Sure, S. Klein, R. Kinjo, G. Bertrand and G. Frenking, *Chem. Eur. J.,* 2012, **18**, 5676-5692.
6. D. Rottschäfer, B. Neumann, H.-G. Stammler, D. M. Andrada and R. S. Ghadwal, *J. Org. Chem.* 2020, **85**, 14351-14359.
7. M. Marín, J. J. Moreno, C. Navarro-Gilabert, E. Álvarez, C. Maya, R. Peloso, M. C. Nicasio and E. Carmona, *Chem. Eur. J.*, 2018, **25**, 260-272.